



**BABEŞ-BOLYAI UNIVERSITY OF CLUJ-NAPOCA  
FACULTY OF CHEMISTRY AND CHEMICAL ENGINEERING**

**PHYSICO-CHEMICAL CHARACTERIZATION OF SOME  
SUPRAMOLECULAR STRUCTURES FORMED FROM  
BIOLOGICALLY ACTIVE COMPOUNDS**

**Ph.D Thesis**

**SUMMARY**

**Author,**

**ING. CHIM. CSABA-PÁL RÁCZ**

SCIENTIFIC ADVISER,  
UNIV. PROF. DR. MARIA TOMOAI-COTIŞEL

**Cluj-Napoca  
2011**

## TABLE OF CONTENTS

INTRODUCTION.....	1
1. Investigation methods and techniques for supramolecular structures.....	2
1.1. Interfacial tension and pressure.....	2
1.2. Monomolecular film balance (LBT).....	7
1.2.1 Insoluble biosurfactant films spread on liquid surfaces.....	7
1.2.2 Compression isotherms.....	8
1.2.3 Orientation of biomolecules at the air/water interface.....	10
1.2.4. Surface compressibility.....	12
1.2.5. Langmuir-Blodgett films ( LB).....	14
1.2.6. KSV 5000 equipment.....	14
1.3 Microscopy methods.....	19
1.3.1 Electron microscopy.....	19
1.3.1.1 Transmission electron microscope (TEM).....	20
1.3.1.2 Scanning electron microscopy (SEM).....	23
1.3.1.3 Atomic force microscopy (AFM).....	25
1.4 Differential Scanning Calorimetry (DSC).....	28
1.5 UV-VIS spectroscopy.....	29
1.6 FTIR spectroscopy.....	31
1.7 Structure determination by X-ray diffraction.....	35
1.7.1 X-ray diffraction.....	35
1.7.2 Structure factor.....	37
1.7.3 Determination methods of crystallographic structure.....	39
1.7.4 Obtaining the structural model from powder diffractogram.....	40
1.7.4.1. The indexing problem.....	40
1.7.4.2. Methods to obtain the structural model.....	41
1.7.4.3. Rietveld refinement of the structural model.....	42
1.7.5 Equipment and mode of operation.....	44
1.8 Literature.....	48
2. Formation and physicochemical characterization of sodium cholate micelles in two-phase systems.....	52
2. 1 Relations between chemical structure and surface properties in systems containing sodium cholate.....	52
2. 2 Critical micelle concentration (CMC) of sodium cholate.....	53
2.2.1 Obtaining the sodium cholate solution.....	53
2.2.2 Measuring methods for critical micelle concentration.....	53
2.2.3 Determination of critical micelle concentration in systems containing sodium cholate.....	54
2.3 Thermodynamic parameters for sodium cholate micellization.....	57
2.3.1 Deduction of thermodynamical parameters.....	57
2.3.2 Preparing of subphases.....	58
2.3.3 Methods to determine interfacial tension.....	59
2.3.4 Determination of thermodynamic parameters for sodium cholate adsorption at the benzene/water interface.....	59
2.4 Conclusions.....	65
2.5 Literature.....	65

3. Kinetic study of the self assembly reaction of some biologically active molecules at the liquid/liquid interface.....	67
3.1 Theoretical models of adsorption.....	68
3.1.1 Diffusion controlled adsorption kinetics.....	68
3.1.2 Langmuir adsorption kinetics.....	69
3.2 Interface tension and adsorption.....	70
3.2.1 Dynamic interfacial tensions.....	71
3.2.2 Elaboration of a new equation for diffusion controlled.....	76
3.2.3 Adsorption dynamics of dibucaine, tetracaine and stearic acid at the benzene/water interface.....	80
3.3 Adsorption mechanism at the oil/water interface.....	85
3.4 Conclusions.....	88
3.5 Literature.....	89
4. Molecular structure and monolayer properties: modeling and experiment.....	92
4.1 Surface characteristics of some carotenoids spread at the air/water interface. Experimental and computational approach.....	92
4.1.1 Preparation of carotenoid films.....	92
4.1.2 HMO and SCF-MO (AM 1 and PM3) calculation. Dipole moments.....	94
4.1.2.1 HMO calculations.....	94
4.1.2.1.1 Energy levels obtained.....	95
4.1.2.1.2 Delocalization degree of the $\pi$ bonds.....	97
4.1.2.1.3. Electron charge density and internuclear distances.....	97
4.1.2.1.4 Dipole moments from HMO data.....	99
4.1.2.2 SCF MO calculations.....	101
4.1.3 Description of compression isotherms.....	103
4.1.4 Molecular geometry. Packing in the monolayer.....	104
4.2 Physicochemical characterization of dipalmitoyl phosphatidylcholine (DPPC) films on aluminum substrate.....	110
4.2.1 Compression isotherms.....	111
4.2.2 Phases structures in DPPC Langmuir films investigated by AFM.....	113
4.2.2.1 Preparation of LB samples.....	113
4.2.2.2 Analysis of the AFM images.....	113
4.2.2.2.1 LB films of pure DPPC.....	114
4.2.2.2.2 Mixed DPPC and P films.....	118
4.3 Conclusions.....	122
4.4 Literature.....	123
5. Preparation and physicochemical characterization of supramolecular structures from noble metals and biologically active compounds.....	126
5.1 Functionalization of noble metals nanoparticles.....	126
5.2 Preparation of noble metals colloidal solutions.....	128
5.2.1 Preparation of gold colloidal solution.....	128
5.2.2 Preparation of silver colloidal solution.....	128
5.3 Physicochemical characterization methods for systems containing gold nanoparticles.....	129
5.3.1 Characterization of the colloidal gold solution.....	130
5.3.1.1 TEM images.....	130
5.3.1.2 UV-VIS spectra.....	131
5.3.2 Interactions with amino acid solutions.....	131
5.3.2.1 UV-VIS spectra.....	131

5.3.2.2	TEM images .....	138
5.3.2.3	AFM images.....	138
5.4	Physicochemical characterization methods for systems containing silver nanoparticles.....	142
5.4.1	Characterization of the colloidal silver solution.....	142
5.4.1.1	UV-VIS spectra.....	142
5.4.1.2	TEM images.....	142
5.4.2	Interaction of the silver sol with $\alpha$ -lipoic acid.....	143
5.4.2.1	UV-VIS spectra.....	144
5.4.2.2	TEM images.....	144
5.5	Conclusions.....	145
5.6	Literature.....	146
6.	Self-assembly of globular or fibrous proteins.....	150
6.1	The major storage protein (PAC) from aleurone cells of barley.....	150
6.1.1	About the storage protein, PAC.....	150
6.1.2	Samples preparation and investigation.....	151
6.1.3	PAC protein characterization.....	152
6.2	Systems formed from bovine serum albumin and melatonin. Simulation of interfacial phenomena at biomembrane level.....	156
6.2.1	About melatonin and bovine serum albumin.....	156
6.2.2	Samples preparation and investigation.....	157
6.2.3	Specific molecular interactions between bovine serum albumin and melatonin.....	157
6.3	Morphology of collagen and anti-cancer drugs assemblies on mica.....	160
6.3.1	About collagen and anti-cancer drugs.....	160
6.3.2	Samples preparation and investigation.....	162
6.3.3	Morphology of collagen and anti-cancer drugs.....	163
6.4	Conclusions.....	168
6.5	Literature.....	170
7.	Chemical and morphological structure of starch granules.....	173
7.1	Chemical characterization.....	173
7.2	Structural and morphological characterization.....	174
7.2.1	AFM imaging.....	174
7.2.1.1	Preparation of AFM samples.....	174
7.2.1.2	AFM images.....	175
7.2.2	SEM imaging.....	184
7.2.2.1	Preparation of SEM samples.....	184
7.2.2.2	SEM images.....	184
7.3	Conclusions.....	187
7.4	Literature.....	188
8.	Formation and physicochemical characterization of supramolecular structures formed from biologically active compounds.....	190
8.1	Supramolecular structures formed from quercetin and $\beta$ -cyclodextrin.....	190
8.1.1	Preparation of the inclusion complex formed from quercetin and $\beta$ -cyclodextrin .....	193
8.1.1.1	Preparation methods.....	193
8.1.2	Methods for physicochemical characterization.....	195
8.1.2.1	Characterization of the inclusion complex of quercetin with $\beta$ -cyclodextrin.....	197

8.1.2.1.1. FTIR spectroscopy .....	197
8.1.2.1.2. Differential Scanning Calorimetry (DSC) .....	199
8.1.2.1.3 X-ray powder diffractometry.....	202
8.1.2.1.4 Determination of the cristallinity degree.....	203
8.1.2.2. The inclusion complex and the supramolecular assembly geometry....	206
8.1.3. Morphology and structure.....	209
8.1.4 Conclusions.....	214
8.1.5 Literature.....	215
8.1.6. Formation thermodynamics of the inclusion complex of $\beta$ -cyclodextrin with quercetin.....	218
8.1.6.1. The equilibrium constant from spectroscopic UV-VIS data.....	218
8.1.6.2. Experimental estimation of the equilibrium constant.....	219
8.1.6.3. Thermodynamic characteristics of the complexation of $\beta$ -cyclodextrin and quercetin.....	232
8.1.6.4. Conclusions.....	232
8.1.6.5. Literature.....	232
8.2. Supramolecular structures formed from $\beta$ -cyclodextrin and $\alpha$ -lipoic acid.....	235
8.2.1. Preparation of the solid complex by coprecipitation.....	236
8.2.2. Methods for the characterization of the inclusion complex formed from $\alpha$ - lipoic acid and $\beta$ -cyclodextrin.....	236
8.2.2.1. Infrared spectroscopy.....	236
8.2.2.2. Differential Scanning Calorimetry.....	237
8.2.2.3. X-ray diffractometry.....	237
8.2.3. Physicochemical characterization of the inclusion complex formed from lipoic acid and $\beta$ -cyclodextrin.....	237
8.2.3.1 Conclusions.....	240
8.2.3.2 Literature.....	240
8.2.4 Structure of the crystal lattice formed by the inclusion complex of lipoic acid with $\beta$ -cyclodextrin.....	242
8.2.4.1 The inclusion complex lipoic acid - $\beta$ -cyclodextrin.....	242
8.2.4.2. Determination of the crystal structure of the inclusion complex $\beta$ -CD-LA. ....	243
8.2.4.2.1 Indexing and model building. ....	243
8.2.4.2.2 Rietveld refinement of the crystal structure model.....	244
8.2.4.3. Molecular packing and hydrogen bonds in the inclusion complex $\beta$ -CD - lipoic acid (1:1) .....	246
8.2.4.4. Mode of inclusion and guest conformation.....	249
8.2.4.5. Conclusions.....	253
8.2.4.6. Literature.....	253
9. General conclusions.....	255
10. Dissemination of scientific results .....	262
10.1 Original scientific papers and books published.....	262
10.2 Participation in national and international conferences and symposia.....	264
General literature.....	266

## INTRODUCTION

The chemistry of supramolecular structures was very suggestively defined by a first leader pomotor in this field, Jean-Marie Lehn, Nobel Prize laureate in 1987, as follows: “the chemsirty of molecular assemblies and of intermolecular bond”. Initially supramolecular compounds were considered only structures of “host-guest” type, nowadays in this category are included molecular devices and machines, structures formed by self assembly and self-organization and the field can not be clearly separated from that of the nanoparticles.

The purpose of scientific research presented in this PhD Thesis is to „capture” molecular information, investigating by various physicochemical methods (**chapter 1**) diverse supramolecular systems formed by the self-assembly of biological active molecules (**chapters 2-9**).

Both the selected biological active molecules and the study methods used were very manifold, trying to cover areas of scientific interest as „hot” as possible. Thus in **chapter 2** micellization was studied in two-phase systems containing sodium cholate and their behavior at the liquis-liquid interface. Other investigated biological active molecules were stearic acid and local anesthetics, dibucaine and tetracaine (**chapter 3**). The study of self-organization of these molecules at the liquid-liquid interface made it possible to deduce mechanism of formation of the molecular suprastructures known in literature as Gibbs films. **Chapter 4** includes the study of nanostructures formed from carotenoids at the air-water interface and from dipalmitoyl phosphatidylcholine on aluminum support. In **chapter 5**, by the study of amino acids and  $\alpha$ -lipoic acid interaction with noble metal (such as gold and silver) nanoparticles, we purposed the modeling of supramolecular structures which may be generated by the contact of living matter with noble metals. Supramolecular structures formed from vegetable or animal proteins by interaction with hormones and anticancer drugs were discussed in **chapter 6**. Morphology and structure of natural aggregates in starch was studied by means of AFM in **chapter 7**. **Chapter 8** deals with structures formed by “host-guest” reactions between  $\beta$ -cyclodextrin and quercetin, as well as between  $\beta$ -cyclodextrin and  $\alpha$ -lipoic acid.

Supramolecular structures develop without implying the dissociation or formation of covalent bonds (**general conclusions**, in **chapter 9**). A large number (**12**) of physicochemical

methods and techniques were used; they are summarized in **chapter 1** and described in **four specialty books**, having the author of this Ph.D. Thesis as co-author (**Chapter 10**). The original research included in the Ph.D. Thesis were published in **15 articles**, **13** of them in **ISI quoted journals (chapter 10)**.

## KEYWORDS

Nanostructured supramolecular systems

Biologically active compounds

Fluid interfaces

Self-organization in monolayers

Self-organization in aqueous phase

Thin films

## 2. FORMATION AND PHYSICOCHEMICAL CHARACTERIZATION OF SODIUM CHOLATE MICELLES IN TWO-PHASE SYSTEMS

### 2.1 RELATIONS BETWEEN CHEMICAL STRUCTURE AND SURFACE PROPERTIES IN SYSTEMS CONTAINING SODIUM CHOLATE

Because of their molecular structure (Fig.2.1.1), bile salts have a polar surface with hydrophilic groups, i.e. hydroxyl, and non-polar surface, containing hydrocarbon segments of the rigid, non-polar steroidal core and a carboxylate group. As shown, the molecule contains three hydroxyl groups, on the same side of the molecule and they form a triangle in the hydrophilic area of the steroidal core. The distance between these three OH groups is 5 Å.

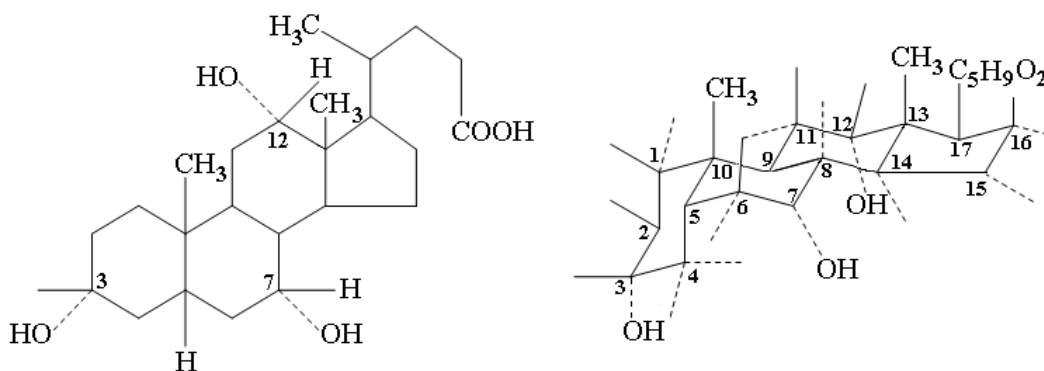


Fig. 2.1.1. Molecular structure of cholic acid (3, 7, 12- trihydroxycholanoic acid)

### 2.2 CRITICAL MICELLE CONCENTRATION (CMC) OF SODIUM CHOLATE

#### 2.2.3 Determination of critical micelle concentration in systems containing sodium cholate

Values of the interfacial tension ( $\sigma$ ), at the carbon tetrachloride/water interface, determined using the pendant drop method [3, 4], are presented in fig.2.2.1, versus the logarithm of NaC concentration. From the intersection of the two linear portions, the CMC can be evaluated.

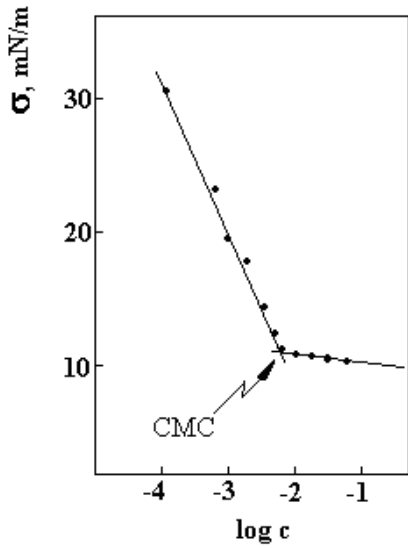


Fig.2.2.1. Interfacial tension ( $\sigma$ ) measured using the pendant drop method versus the logarithm of NaC concentration

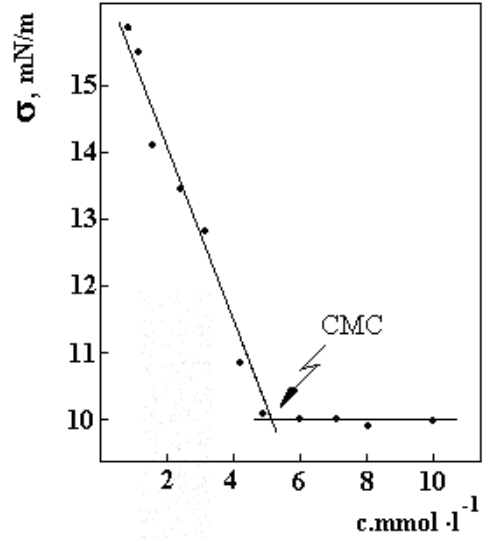


Fig.2.2.2. Interfacial tension ( $\sigma$ ) using the Wilhemy method, versus NaC molar concentration ( $c$ )

The plot of equivalent conductance ( $\Lambda$ ) vs.  $\sqrt{c}$ , the square root of the NaC concentration, is given in fig. 2.2.3. As shown, at the CMC there is a sudden change of slope. Turbidity ( $\tau$ ) versus analytical NaC concentration is presented in figure 2.2.4. There are two linear portions, their intersection being at CMC.

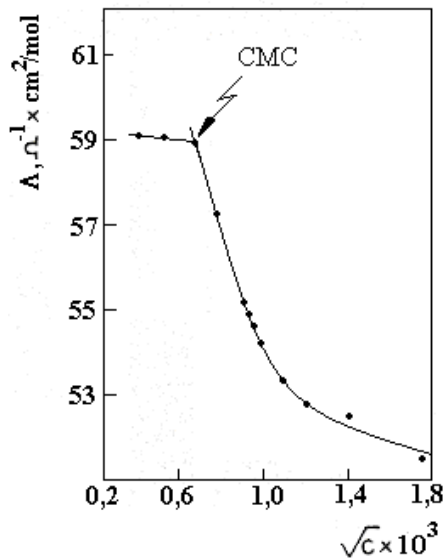


Fig. 2.2.3. Equivalent conductance ( $\Lambda$ ) vs.  $\sqrt{c}$  NaC

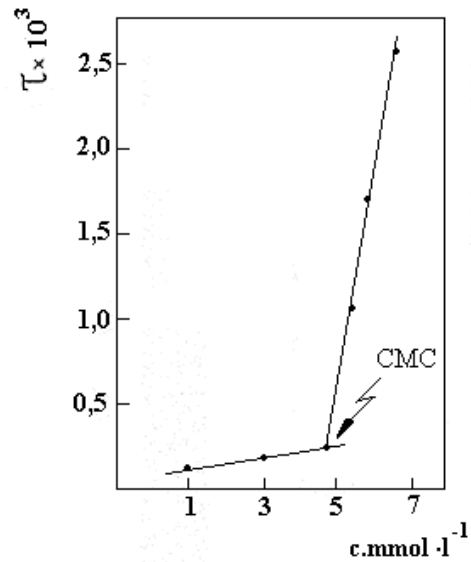


Fig.2.2.4. Turbidity ( $\tau$ ) versus molar NaC concentration

The CMC values deduced from our experimental data are presented in Table 2.2.1. In this table are also given data from literature. From these, the adsorption maximum was calculated and the molecular area values, given in Table 2.2.2.

**Table 2.2.1. CMC values for aqueous NaC solutions**

Method	temperature	CMC	References
	(°C)	(mM/l)	
Drop volume	22	5.55	[123]
Plate	20	5.31	[124]
Conductometric	23	5.18	[123]
Turbidimetric	22	4.91	[123]
Light diffusion	20	20	[94]
Solubilisation	20	13	[92]
Surface tension	20	5	[96]
Surface tension	22	4.9	[90]
Surface tension	22	3.25	[90]

**Table 2.2.2 Adsorption maximum and molecular area of NaC at liquid/liquid interface**

Interface	$\Gamma_m \times 10^{10}, mol \cdot cm^{-2}$	$A_0, \text{Å}^2/\text{molecule}$
CCl <sub>4</sub> /water	1.92	86.8
Benzene/water	1.05	158.4

## 2.3 THERMODYNAMIC PARAMETERS FOR SODIUM CHOLATE MICELLIZATION

### 2.3.1 Deduction of thermodynamic parameters

The interfacial tension ( $\sigma$ , mN/m) at the benzene/aqueous surfactant solution interface was measured against temperature for several surfactant concentrations, around the critical micelle concentration (CMC). We obtained thermodynamic parameters which characterize both surfactant adsorption and its micellization

#### **2.3.4 Determination of thermodynamic parameters for sodium cholate adsorption at the benzene/water interface**

From the values of interfacial tension plotted against temperature and concentration, we could evaluate the entropy variation corresponding to the adsorption per mol of surfactant ( $\Delta s/\Gamma_1$ , adsorption entropy). This quantity presents positive values and greatly decreases at  $m_1 < \text{CMC}$ . This discontinuity at CMC, indicates at 298 K a rather low micellization entropy. At higher temperatures, the micellization entropy becomes negative.

It was found that collate geometry and hydrophilicity have a significant effect on the properties of adsorbed films of sodium cholate and on the behavior of micelles formation.

### 3. KINETIC STUDY OF THE SELF ASSEMBLY REACTION OF SOME BIOLOGICALLY ACTIVE MOLECULES AT THE LIQUID/LIQUID INTERFACE

One of the objectives of this study is to develop a kinetic model and to apply it to the adsorption of biologically active compounds, for example, two local anesthetics (tetracaine and dibucaine) from aqueous solutions at the interface with pure benzene. A major objective of this research is to elucidate the adsorption of another biologically active compound, i.e. a fatty acid (stearic acid) from the organic phase (benzene) to the interface with water, stearic acid being considered a simple model of lipid compound.

#### 3.2.1 Dynamic interfacial tensions

The values of dynamic interfacial tensions for the adsorption of the two anesthetics at the benzene/water interface, along with the equilibrium values, are given in Table 3.1.

**Table 3.1.** Dynamic interfacial tensions (mN/m) at the benzene/water interface

Anesthetics t, min	Dibucaine			Tetracaine		
	C <sub>o</sub> , mol dm <sup>-3</sup>					
	0.001	0.005	0.010	0.001	0.005	0.010
1	31.9	28.7	26.4	32.8	31.1	29.9
2	31.1	27.1	24.3	31.9	30.5	28.9
3	30.2	25.4	22.2	31.7	29.2	27.5
4	29.7	24.6	20.8	31.3	28.7	27.0
5	29.2	23.5	20.0	31.1	28.2	26.2
6	28.8	23.1	19.2	30.8	27.7	25.9
7	28.4	22.1	18.6	30.7	27.5	25.3
8	28.1	21.9	18.2	30.5	27.2	25.1
9	27.8	21.2	17.5	30.3	27.0	24.7
10	27.5	20.9	17.3	30.1	26.7	24.5
11	27.3	20.4	16.8	30.0	26.6	24.3
12	27.0	20.1	16.6	29.9	26.4	24.0
13	26.9	19.7	16.2	29.8	26.3	23.9
14	26.6	19.4	16.0	29.6	26.1	23.8
15	26.5	19.2	15.8	29.5	26.0	23.7
∞	26.0	18.6	15.6	29.3	25.6	23.3

In order to test the validity of the kinetic equation (3.7) [177], the left side of the equation (denoted by  $y$ ) was calculated, using the experimental  $\sigma$  values presented in Tab. 3.1, as well as their equilibrium values  $\sigma_e$ , corresponding to  $t = \infty$ , and taking  $\sigma_o = 34.7 \text{ mN/m}$ . Using the kinetic equations, values of the relative adsorption and desorption constants, given in Tab. 3.3, were evaluated.

**Table 3.3.** Relative adsorption and desorption constants

Biocompound	$k_1/\Gamma_\infty$ $\text{dm}^3 \text{ mol}^{-1} \text{ min}^{-1}$	$k_2/\Gamma_\infty$ $\text{min}^{-1}$	r	$k_1/k_2$ $\text{mol}^{-1} \text{ dm}^3$
Dibucaine	7.250	0.1590	0.9914	45.6
Tetracaine	4.990	0.1490	0.9988	33.5
Stearic acid	0.212	0.0392	0.9990	5.4

For a better correlation of experimental data we proposed a new theoretical model and a new kinetic equation, based on the diffusion equation of Ward and Tordai, associated with the dimensional van der Waals equation of state [177].

### 3.3 ADSORPTION MECHANISM AT THE OIL/WATER INTERFACE

To provide a better picture of the mechanism of adsorption, we represented in Fig. 3.14 the variation of energy ( $E$ ) against distance to the interface ( $Z$ ) and illustrated the energy barriers for adsorption and desorption process at liquid-liquid interface.

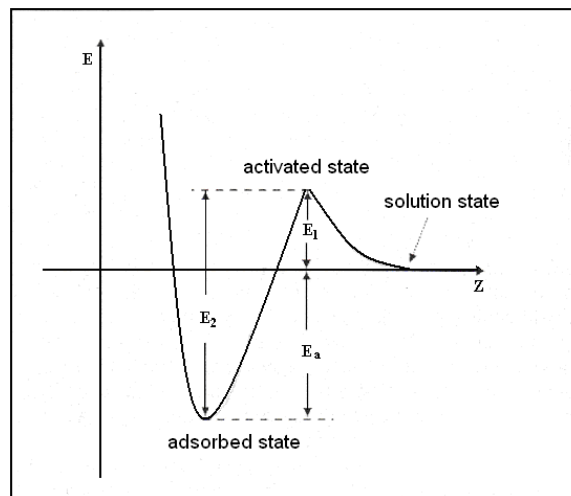


**Fig.3.14** Relation between adsorption barrier  $E_1$  (i.e. the adsorption activation energy), desorption barrier  $E_2$  (i.e. the desorption activation energy) and adsorption energy ( $E_a$ )

Driving forces for the adsorption of anesthetics (water-soluble molecules) are hydrophobic interactions between the penetrated hydrophobic chains and the oil phase, which are accompanied by an increase of system entropy caused by the destruction of the ordered structure of water molecules, formed around the hydrophobic chains in the aqueous phase.

On the contrary, the driving force for adsorption of stearic acid (a component practically insoluble in water) is the change in system enthalpy due to hydration of the hydrophilic polar head group when immersed in aqueous phase [190].

## 4. MOLECULAR STRUCTURE AND MONOLAYER PROPERTIES: MODELING AND EXPERIMENT

Monolayer characteristics were determined for three carotenoid pigments (Fig. 4.1.1) [207, 208].

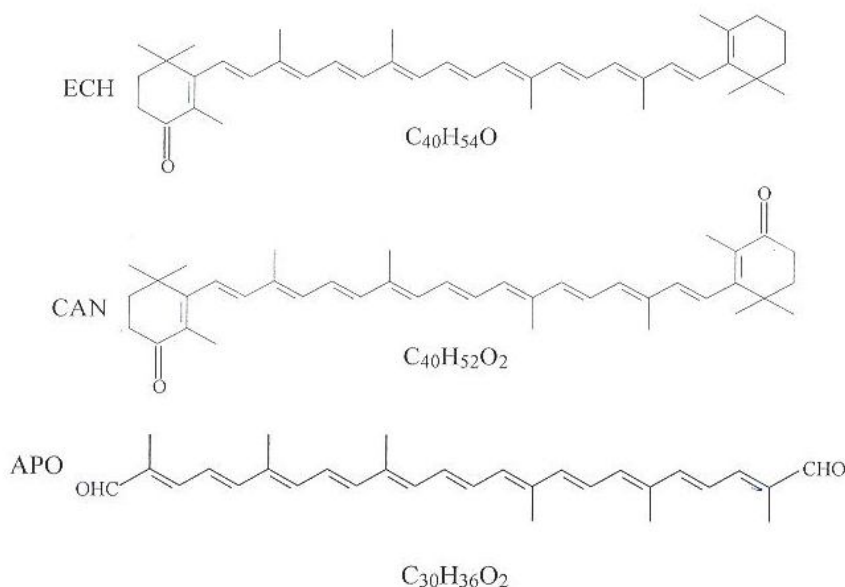


**Figure 4.1.1** Molecular structure of carotenoids:  $\beta$ , $\beta$ -carotene-4-on (echinenone, ECH),  $\beta$ , $\beta$ -carotene-4,4'-dione (canthaxanthin, CAN) and 4,4'-diapo- $\psi$ ,  $\psi$ -carotene-4,4'-dial (also called 4,4'-diapolyconepenedial, APO)

### 4.1.2 HMO and SCF-MO (AM 1 and PM3) calculation. Dipole moments

#### 4.1.2.1.4 Dipole moments from HMO data

We used simple HMO calculations for the delocalized  $\pi$  electron system of the three molecules [207]. From the  $\pi$  electron densities and bond orders dipole moments for different bonds were estimated, based on logical assumptions. While for CC bonds only  $\pi$  dipole moments were considered, for CO bonds a  $\sigma$  component was also included. These dipole moments of individual bonds were vectorially composed (see Fig.4.1.9 for the composition of dipole moments for the first three bonds), beginning with the CO bond, which is supposed to be horizontally disposed directly on the water substrate, while assuming the bond angles in the conjugated system to be  $120^\circ$  (trigonal hybridization for all C and O atoms).

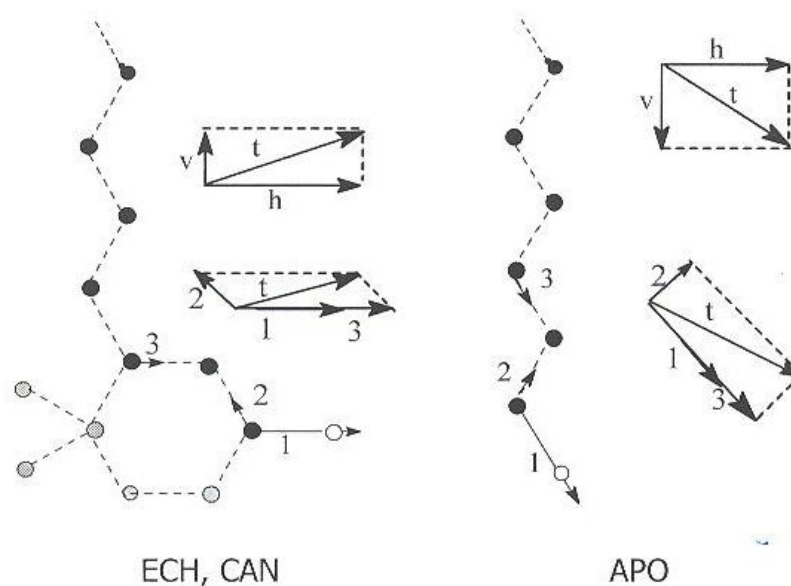


**Figure 4.1.9.** Composition of dipole moments for the first 3 bonds and the decomposition of the total dipole moment into horizontal and vertical components. Symbols: black circles – C ( $sp^2$ ) atom, gray circles - C ( $sp^3$ ) atom, white circles O ( $sp^2$ ) atom.

#### 4.1.2.2 SCF MO calculations

More complex MO calculations were executed, involving all electrons ( $\sigma$  and  $\pi$ ) for the three carotenoids (ECH, CAN and APO), all in *all-trans* form. The calculations were performed at the restricted Hartree-Fock (RHF) level using two semi-empirical SCF MO methods: Austin Model 1, AM1 [24] and the Parametric Model PM3, by means of HyperChem 7.5 software package. They were also used to estimate the dipole moments.

#### 4.1.3 Description of compression isotherms

Compression isotherms were recorded for the three carotenoids (ECH, CAN and APO) spread at the air/water interface (Fig.4.1.10). Starting with these compression isotherms, surface characteristics were determined, namely: the collapse pressure  $\pi_c$ , surface compression modulus  $C_s^{-1}$ , and interaction parameters  $A'_o$  (Table 4.1.1).

#### 4.1.4 Molecular geometry. Packing in the monolayer

The horizontal component of the dipole moment for the first three bonds in the conjugated system  $\mu_{h3}$ , i.e. the dipole moment of the principal group, decreases in the sequence ECH>CAN>APO, similarly with the experimentally established  $\alpha$  and  $C_s^{-1}$  values, where  $\alpha$  is a measure for the intermolecular attraction forces, and  $C_s^{-1}$  the surface compression modulus.

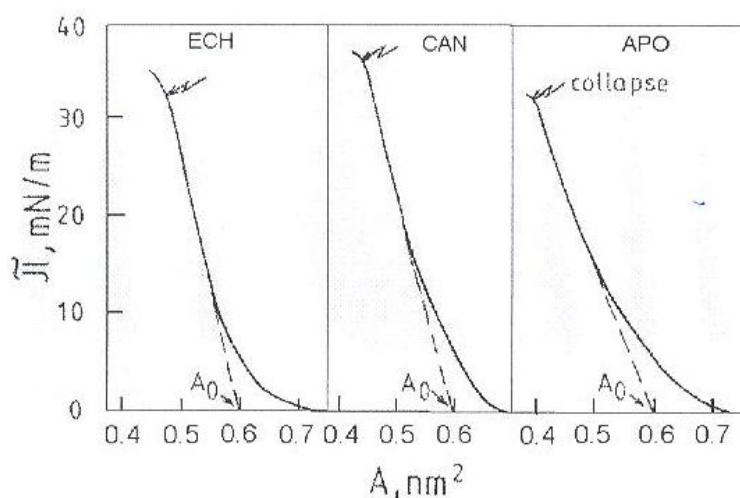


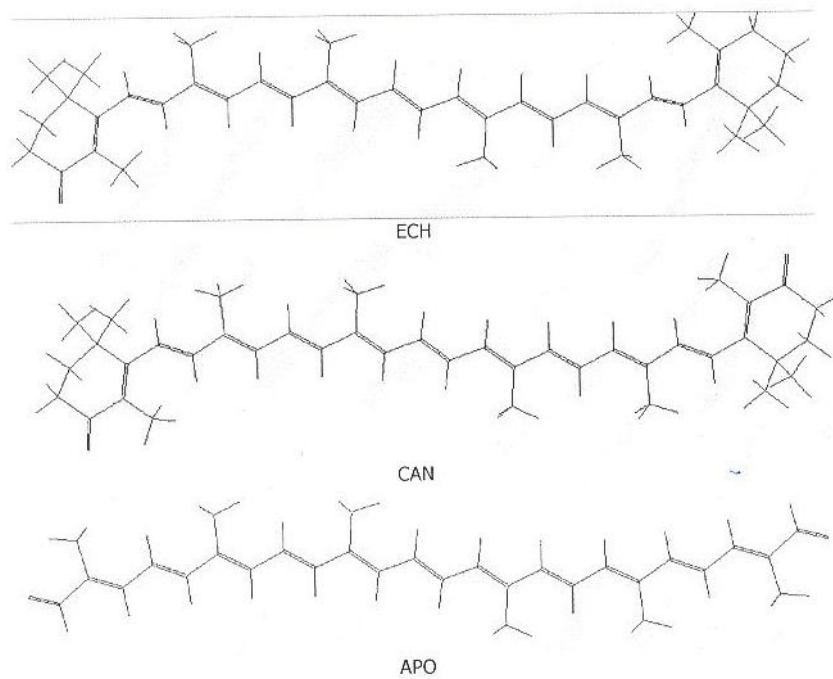
**Figure 4.1.10.** Compression isotherms: surface pressure against molecular area for the carotenoids ECH, CAN and APO

**Table 4.1.1. Surface characteristics of the three investigated carotenoids**

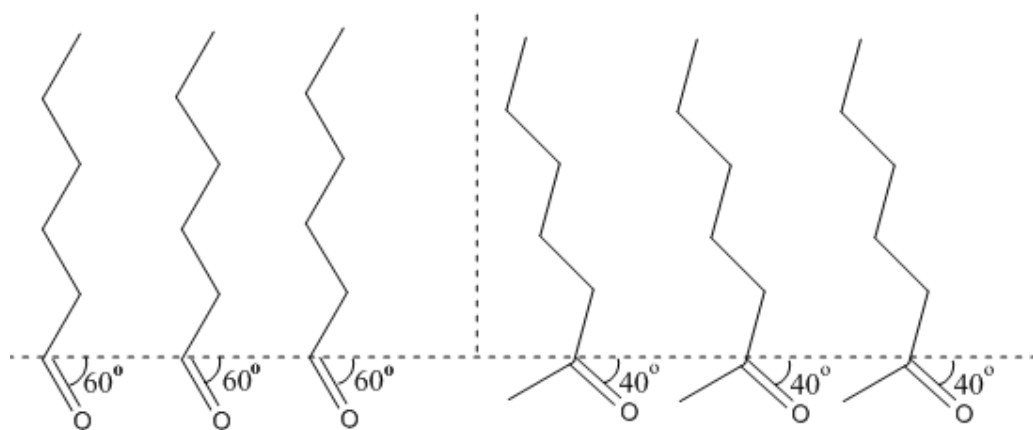
Carotenoid	$\pi_c$ ( $mN \cdot m^{-1}$ )	$C_s^{-1}$ ( $mN \cdot m^{-1}$ )	$\alpha \cdot 10^{30}$ ( $N \cdot m^2$ )	$A_0'$ ( $nm^2$ )
ECH	32	151	9.02	0.438
CAN	36	145	8.74	0.432
APO	32	95	6.71	0.392

Fig.4.1.11. presents the optimized geometries as resulted from PM3 calculations in the plane of the first two inertial axes.

The semi empirical SCF-MO calculations for the three investigated carotenoids give similar results to those from HMO calculations. The dipole moments of the polar groups are correlated with the thermodynamic surface characteristics. For the echinenone (ECH) and canthaxanthin (CAN) molecules, the molecular orientation in the condensed monolayer is considered to be perpendicular to the air/water interface and the monolayer resulted from this molecular packing is rather rigid, while the APO molecules present a different orientation and high compressibility. These molecules are deviated from the vertical position, i.e. inclined in order to decrease the angle of the C=O bond to the air/water interface (Fig. 4.1.15). The angle should be about 40°.



**Figure 4.1.11.** Optimized geometries (PM3 calculation) for the three carotenoid molecules



**Fig. 4.1.15** Orientation of APO molecules at the air/water interface

## 4.2 PHYSICOCHEMICAL CHARACTERIZATION OF DIPALMITOYL PHOSPHATIDYLCHOLINE (DPPC) FILMS ON ALUMINUM SUBSTRATE

For the membrane modelling various models were used, among them dipalmitoyl phosphatidylcholine (DPPC) monolayers, also named nanolayers, lipid vesicles or liposomes, and Langmuir-Blodgett (LB) films, investigated by various techniques: Langmuir technique, Langmuir-Blodgett (LB) technique, associated with atomic force microscopy (AFM). DPPC Langmuir nanolayers in absence or presence of procaine (P) at the air/water interface were investigated using compression isotherms. The Langmuir-Blodgett films transferred on aluminum coated glass support were visualized by atomic force microscopy (AFM), e.g. Fig. 4.2.4 [249, 571]. The analysis of AFM images Analiza imaginilor AFM reveals the differences between the LB film surfaces of pure DPPC, and DPPC with P, suggesting that there is a change in surface composition.

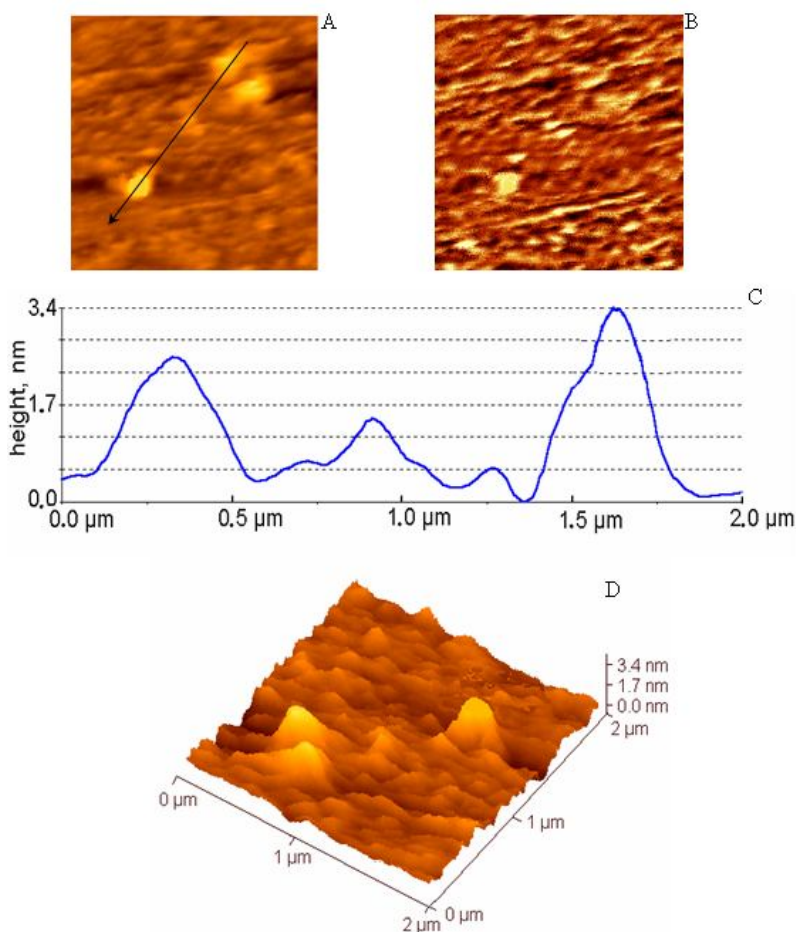


**Fig.4.2.4** AFM images: 2D - topography (A) and phase image (B) of LB films of pure DPPC transferred on aluminum support at the principal phase transition at 8 mN/m; scanned area  $2 \times 2 \mu\text{m}^2$ . C image represents the profile of the cross section along the arrow in image (A). 3D topography (D) of the 2D image (A).

The experimental structures of the LB collapse film visualized by AFM and the profiles of cross sections can be suggestively explained by means of the collapse model by nucleation and nuclei growing. The AFM images of DPPC with P reveal their association in loosely aggregated particles at advanced collapse against the case of pure DPPC film.

Our investigations also showed a long term stability of pure DPPC films and of DPPC films with P transferred on aluminum support. This high stability could involve the interaction between DPPC molecules and between DPPC and P, plus the interaction between the aluminum support and the film forming molecules.

## 5. PREPARATION AND PHYSICOCHEMICAL CHARACTERIZATION OF SUPRAMOLECULAR STRUCTURES FROM NOBLE METALS AND BIOLOGICALLY ACTIVE COMPOUNDS

Colloidal solutions containing gold [328] and silver [329] nanoparticles were prepared..

### 5.3 PHYSICOCHEMICAL CHARACTERIZATION METHODS FOR SYSTEMS CONTAINING GOLD NANOPARTICLES

Both colloidal solutions containing only noble metal nanoparticles, and those where biomolecules were added (amino acids,  $\alpha$ -lipoic acid) were characterized by UV-VIS spectroscopy, transmission electron microscopy (TEM) and AFM.

#### 5.3.2.1 UV-VIS spectra

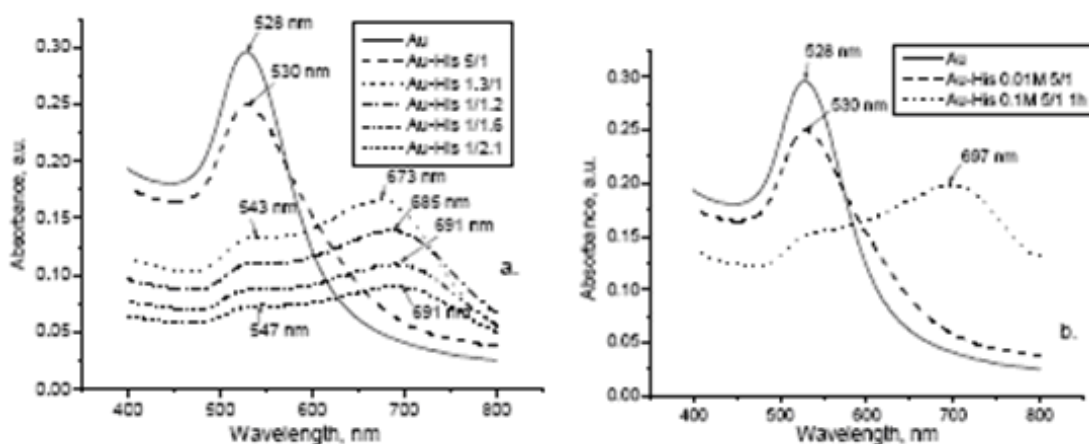


**Fig.5.3.7.** Optical spectra of the colloidal gold solution with 0.01 M histidine solution 0,01 M in various ratios (a) and with histidine solutions of different concentrations (b) [328]

In the UV-VIS spectra we remark the bands characteristic for the surface plasmon resonance (SPR) of metal nanoparticles, and by adding the biomolecules the bands maxima are shifted towards higher wavelengths, while the shift increases with increasing interaction. The self aggregation of nanoparticles mediated by biomolecules causes a broadening of adsorption bands and a pronounced bathochromic shift (Fig. 5.3.7.)

The amino acids bonding to the interface of the gold nanoparticle can occur through the amine function, or for those containing sulfur, by means of this atom.

### 5.4.1.2 TEM images

The TEM images visualize the metal nanoparticles and the aggregates formed by these nanoparticles in presence of biomolecules (Fig. 5.4.6).

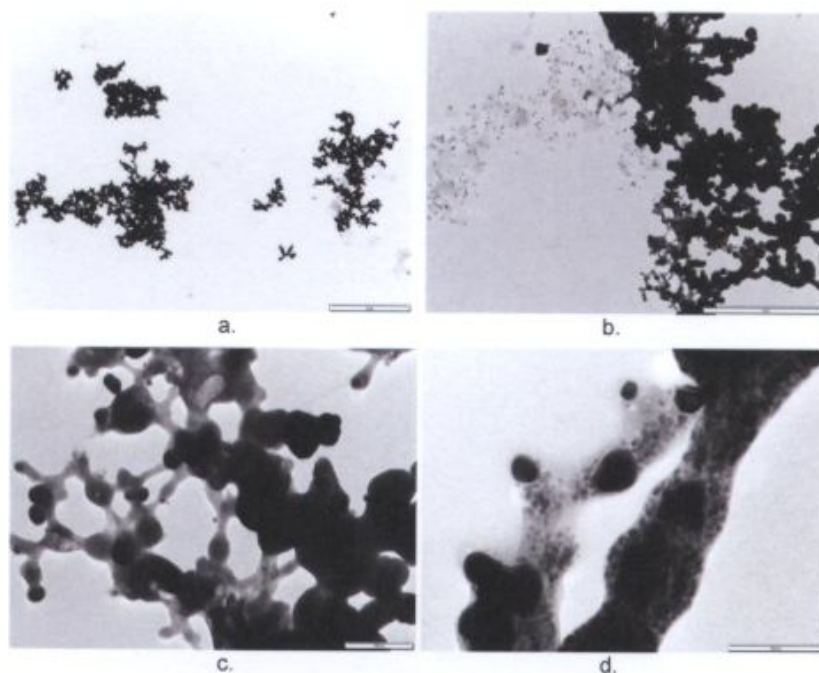


**Fig.5.4.6.** TEM images of silver nanoparticles with  $\alpha$ -lipoic acids. The bars in the images correspond to 5  $\mu\text{m}$  (a), 2  $\mu\text{m}$  (b), 200 nm (c) and 100 nm (d) [329]

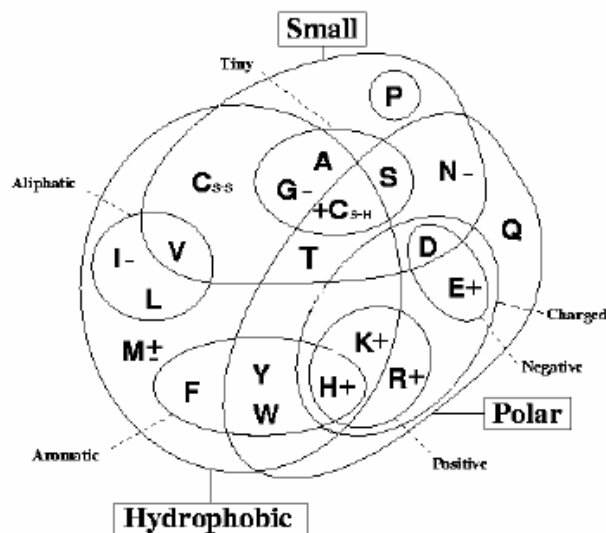


**Fig. 5.3.17.** Venn diagram grouping amino acids according to their properties. A – Alanine  
 CS-H – Cysteine CS-S cystine D – Aspartic acid E – Glutamic acid  
 F – Phenilalanine G – Glycine H – Histidine I – Isoleucine K – Lysine L – Leucine  
 M – Methionine N – Asparagine P – Proline Q – Glutamine R – Arginine S – Serine

In order to rationalize the behavior of the investigated amino acids versus gold nanoparticles we use a Venn diagram (Fig. 5.3.17), grouping amino acids according to their properties. The amino acids found to interact strongly with the gold nanoparticles and to initiate their aggregation were noted with “+”, and those which give only slight shifts of the UV-Vis absorption band with “-“.

A possible model for the binding of an amino acid to the gold nanoparticle and the formation of particles aggregates is presented for cysteine in Fig.5.3.18.

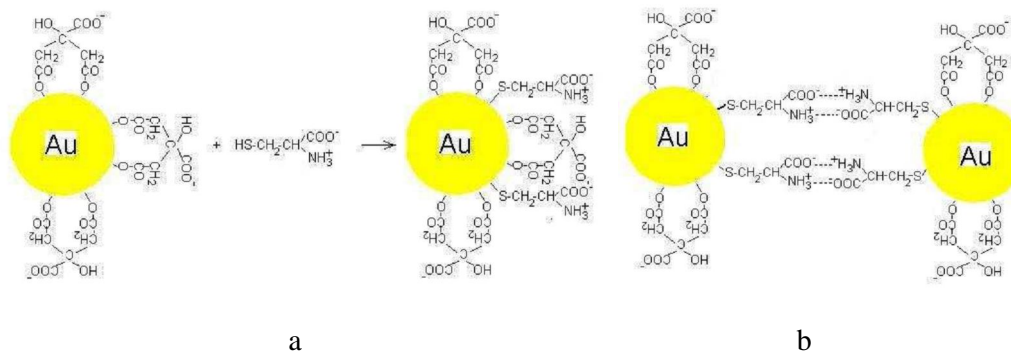


**Fig. 5.3.18.** A model of cysteine binding to citrate capped gold nanoparticles (a) and of bonds formation between gold nanoparticles (b)

## **6. SELF-ASSEMBLY OF GLOBULAR OR FIBROUS PROTEINS**

### **6.1. THE MAJOR STORAGE PROTEIN (PAC) FROM ALEURONE CELLS OF BARLEY**

The aim of this study is to investigate the self assembly of PAC protein layers, adsorbed on solid support. Our attention is mainly directed to the determination of the surface structure of dried protein layers and the apparition of protein nanoparticles within the protein layers. The structure of protein layers adsorbed on glass was studied depending on adsorption time, protein concentration, pH and ionic strength. To our knowledge, this is the first study on PAC protein adsorption on solid support, and includes nanoscale details on the structure of of protein PAC layers [359]. PAC proteina has a unique structure in the film adsorbed on glass support investigated by AFM. A process of this kind of molecular and supramolecular structuration can occur within the vacuoles which store proteins during the development process of cereal grains.

### **6.2 SYSTEMS FORMED FROM BOVINE SERUM ALBUMIN AND MELATONIN. SIMULATION OF INTERFACIAL PHENOMENA AT BIOMEMBRANES LEVEL**

We aim to determine the effects of melatonin on self assembled bovine serum alumin (BSA) films, adsorbed at the air/aqueous solution interface, near the physiological pH [337]. Our experimental data indicate that there are specific interactions between melatonin and BSA. Melatonin increases the interfacial pressure of adsorbed BSA films, exerting a substantial stabilizing effect on the interfacial BSA films, self assembled at the air/water interface. Our results confirm both the involvement of melatonin in specific interactions with BSA, and its notable effect on the stabilization of biological compounds at fluid interfaces.

### **6.3. MORPHOLOGY OF COLLAGEN AND ANTI-CANCER DRUGS ASSEMBLIES ON MICA**

The self assemblies of type I collagen (COL) from bovine Achilles tendon with some anti-cancer drugs, such as 5-fluorouracil (FLU) or doxorubicin (DOX), on mica substrate were investigated by atomic force microscopy (AFM) [576]. The AFM images show the different morphologies of self assemblies made of COL, COL-FLU and COL-DOX. (Fig. 8). The data suggest that the anti-cancer drugs lead to the formation of collagen self

assemblies with a notable level of stability, reflecting a high level of nanometer scale order within the adsorbed layers on mica surface. The interaction of these self assemblies with the mica surface is strong, and the specific interactions between molecules within the self assembled layers could be explained by means of hydrogen bonds, but the simple entrapment of drug molecules into the collagen matrix can not be ruled out.

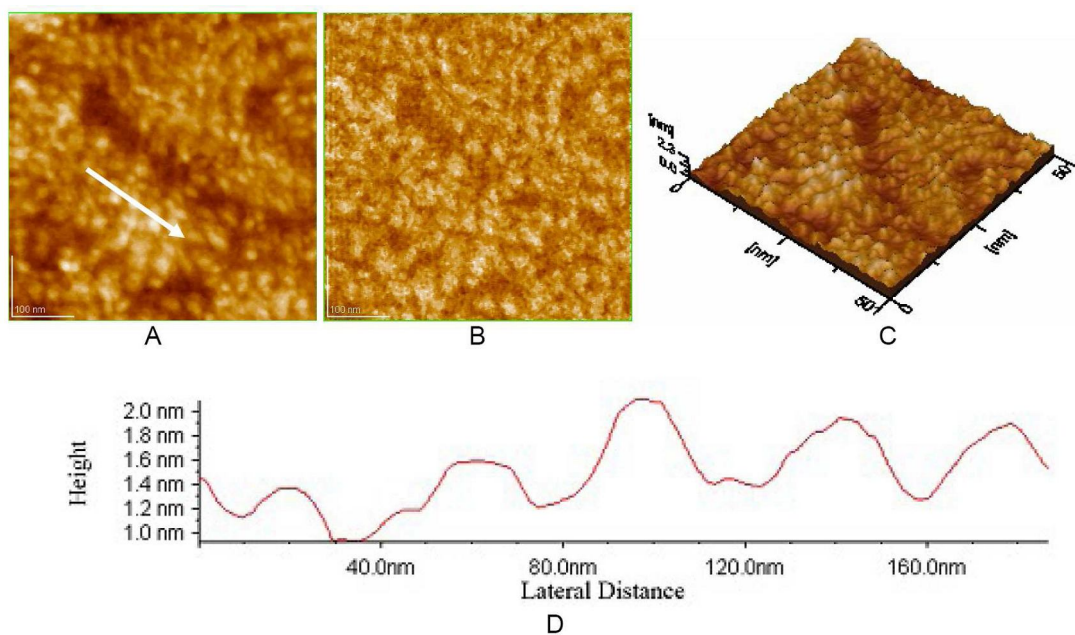


**Figure 8.** Collagen with 5-fluorouracil film on mica. A) 2D – topography; B) phase image; C) 3D-topography; D) profile of the cross section along the arrow in Fig. 8A. Scanned area: 0.5  $\mu\text{m}$  x 0.5  $\mu\text{m}$ .

## 7. CHEMICAL AND MORPHOLOGICAL STRUCTURE OF STARCH GRANULES

### 7.2.1.2 AFM images

Atomic force microscopy (AFM) was used to reveal the micro and nanostructure of maize starch granules from Romanian cultivar [432, 433]. The size, shape and surface morphology of the native maize starch granules are shown by such images. A selection of AFM images of maize starch granules compacted as tablets is shown in Fig. 1, and of those spread out in thin film – in Fig. 7. From the AFM images, 2D topographies (Figure 1a, 7a) și 3D topographies (Figure 1d, 7d), as well as from the phase images (Figure 1b, 7b) and amplitude images (Figure 1c, 7c), we can observe the surface structuration of starch granules, primarily the presence of protrusions (small rounded and elongated nodules or particles).

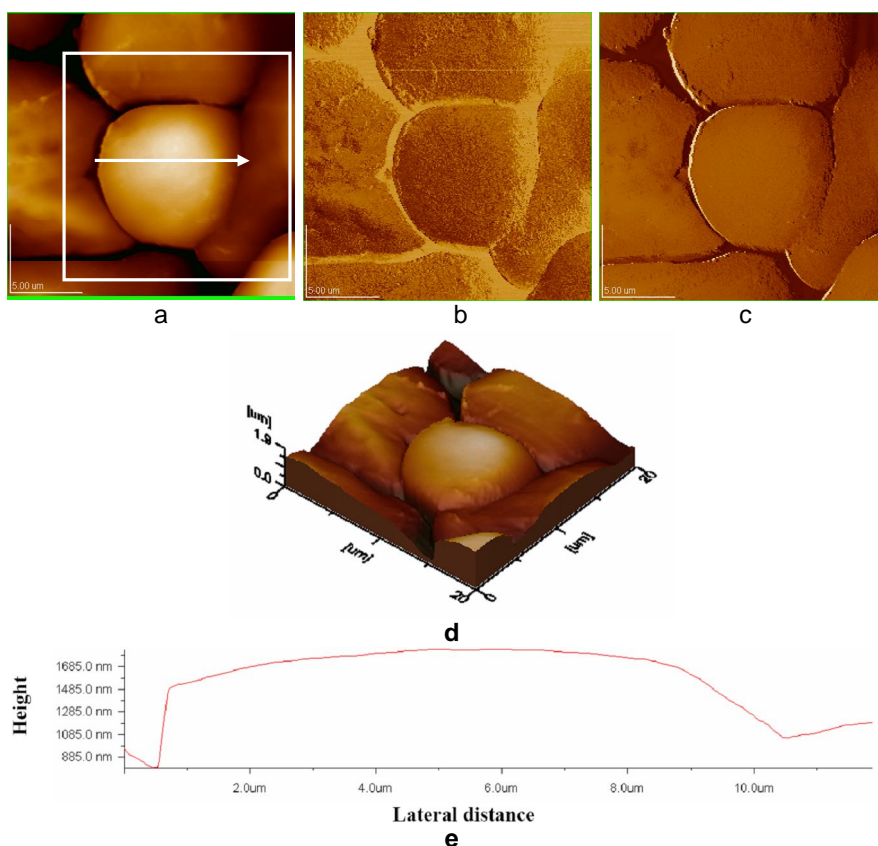


**Figure 1.** AFM images of maize starch compacted as a tablet. Scanned area: 20  $\mu\text{m}$  x 20  $\mu\text{m}$ . a) 2D – topography; b) phase image; c) amplitude image; d) 3D-topography; e) profile of the cross-section along the arrow given in panel a.

The surface structures evidenced by AFM imaging, such as protruding nodules on the surface of the starch granules have various sizes, in a large range of values, from 30 nm to 80 nm. Frequently, fine particles were found to self assemble on the granule surface into rather straight arrangements forming rows.

The surface organization of the starch granule is probably consisting of blocklets as structural elements that have already been proposed for the association and clustering of amylopectin helices within the starch granule and on the granule surface. We suggest that the observed smallest fine particles might also correspond to the individual clusters of amylopectin in substantial agreement with the proposed cluster model and blocklets concept. The existence of rather smooth regions with low surface roughness and rougher zones on the starch granules is confirmed.

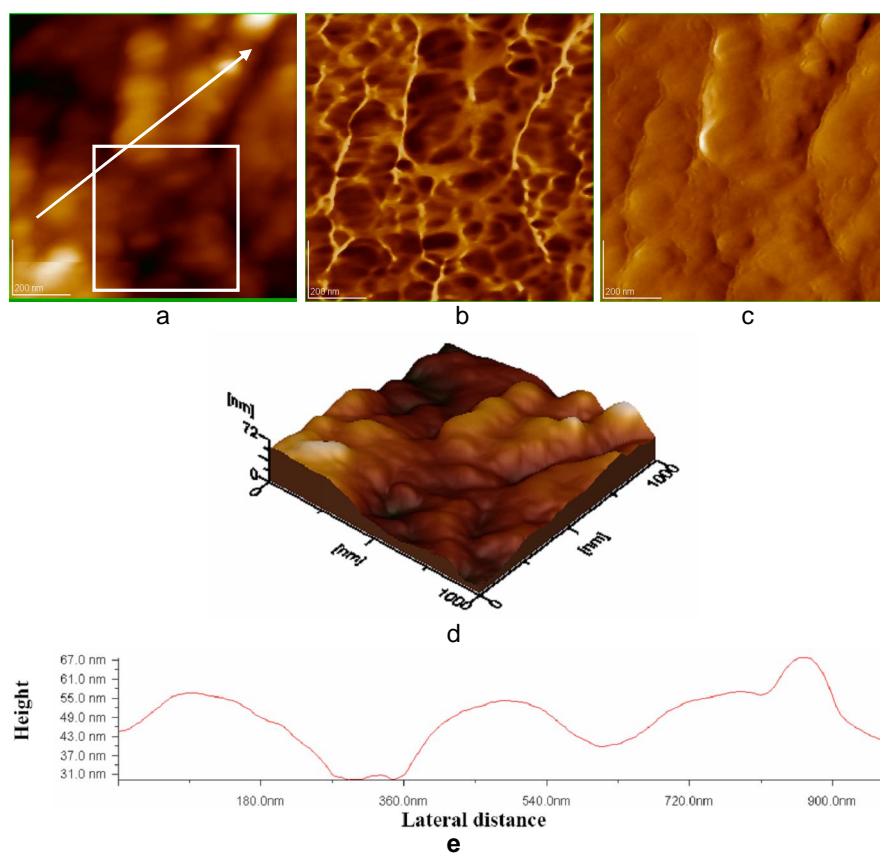


**Figure 7.** AFM images of the maize starch powder spread as a thin film. Scanned area:  $1\ \mu\text{m} \times 1\ \mu\text{m}$ . a) 2D – topography; b) phase image; c) amplitude image; d) 3D-topography; e) profile of the cross section along the arrow in panel a.

## 7.2.2 SEM imaging

### 7.2.2.2 SEM images

Some of the SEM images of the starch granules from potatoes in thin film, examined by the secondary electron imaging (SEI) technique are given in Figure 8 for different measuring areas. The analogous pictures of starch granules from maize are given in Figure 9.

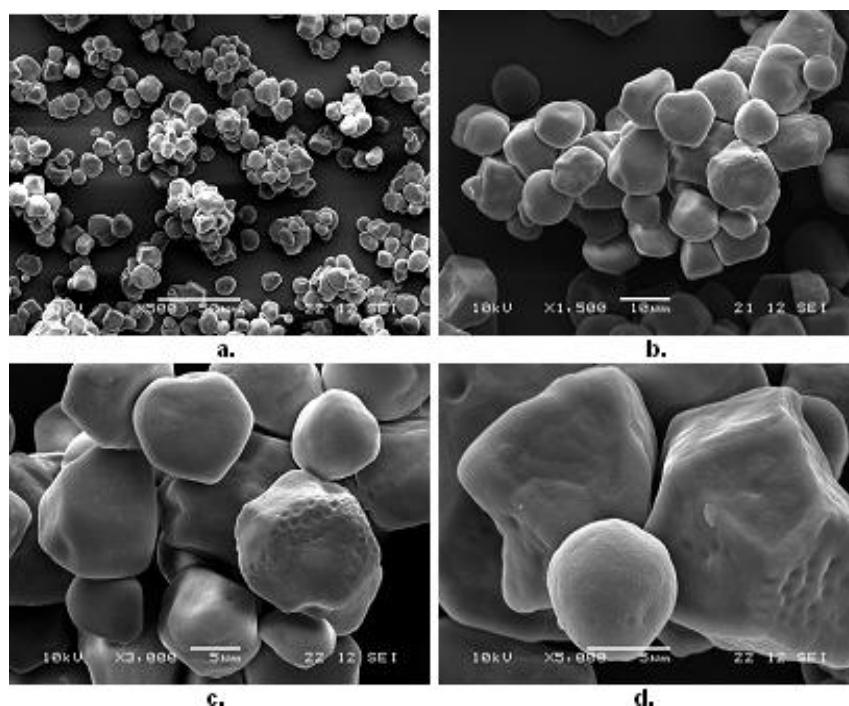


**Figure 8.** Potato starch granules (sample 1) visualized by SEM (SEI technique), the bar lengths are respectively: 50  $\mu\text{m}$  (a); 10  $\mu\text{m}$  (b); 5  $\mu\text{m}$  (c); 5  $\mu\text{m}$  (d).

From the sizes of a great number of particles (some hundreds), measured on the SEM images, the average size (equivalent diameter of the granules) and the standard deviation (SDEV) were calculated, together with the extreme values of the granule sizes. The histograms providing the size distribution of starch granules, obtained from SEM pictures, are given in Figure 10. The size distribution is similar in the two samples, i.e. there are no significant differences between the potato (Fig. 10a) and maize (Fig. 10b) starch granules. From these histograms, the granulometry of the starch samples was derived.

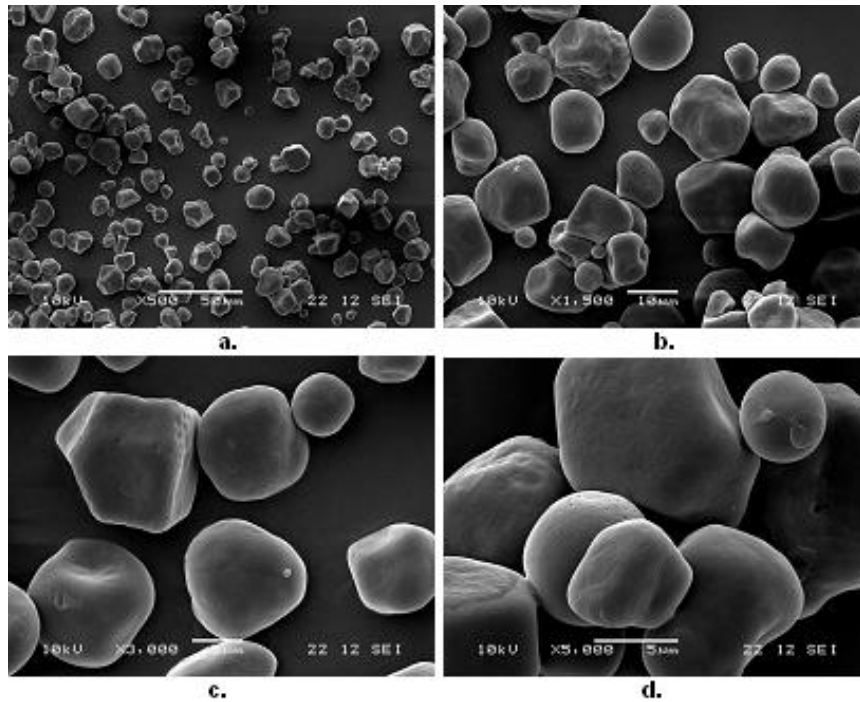


**Figure 9.** Maize starch granules (sample 2) visualized by SEM (SEI technique), the bar lengths are respectively: 50  $\mu\text{m}$  (a); 10  $\mu\text{m}$  (b); 5  $\mu\text{m}$  (c); 5  $\mu\text{m}$  (d).

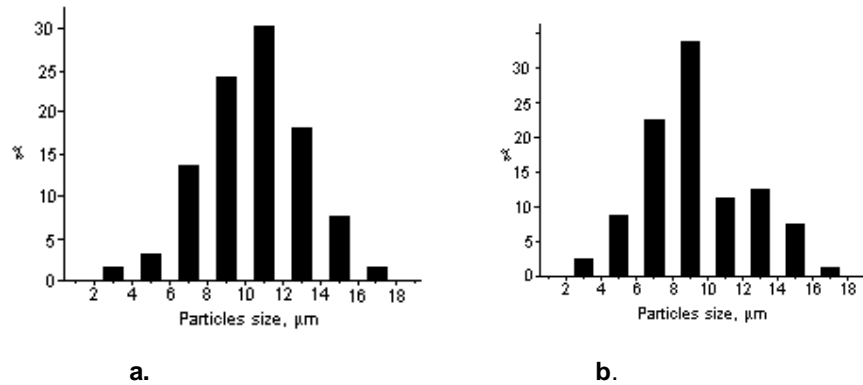


**Figure 10.** Histograms of size distribution of granules in the potato starch sample 1 (a) and the maize starch – sample 2 (b) thin films

Thus, some Romanian starches were investigated for the first time in literature, using SEM imaging, and their granulometry was established from histograms based on the measurement of granules sizes. We could also perform a comparison between the morphology of Romanian starch granules with other kinds of starch published in literature

## 8. FORMATION AND PHYSICOCHEMICAL CHARACTERIZATION OF SUPRAMOLECULAR STRUCTURES FORMED FROM BIOLOGICALLY ACTIVE COMPOUNDS

### 8.1. SUPRAMOLECULAR STRUCTURES FORMED FROM QUERCETIN AND $\beta$ -CYCLODEXTRIN [489-496]

#### 8.1.2 Methods for physicochemical characterization

##### 8.1.2.1. Characterization of the inclusion complex of quercetin with $\beta$ -cyclodextrin

###### 8.1.2.1. 1. FTIR spectroscopy

In the spectral domain given in Fig.8.1.1, the O-H stretching frequency on  $\beta$ -CD, localized at  $3380\text{ cm}^{-1}$ , is shifted to  $3412\text{ cm}^{-1}$  for the *co* and *fd* compounds. Perhaps some hydrogen bonds are broken. It is clear from Fig.8.1.2 that the C = O group is involved in the complexation, its stretching frequency is shifted from  $1664$  to  $1660\text{ cm}^{-1}$  for the *fd* and *co* compounds. This fact points up that the C = O group (ketone group), at C4 of the quercetin framework is involved in hydrogen bonds during the complexation of Q with  $\beta$ -CD.

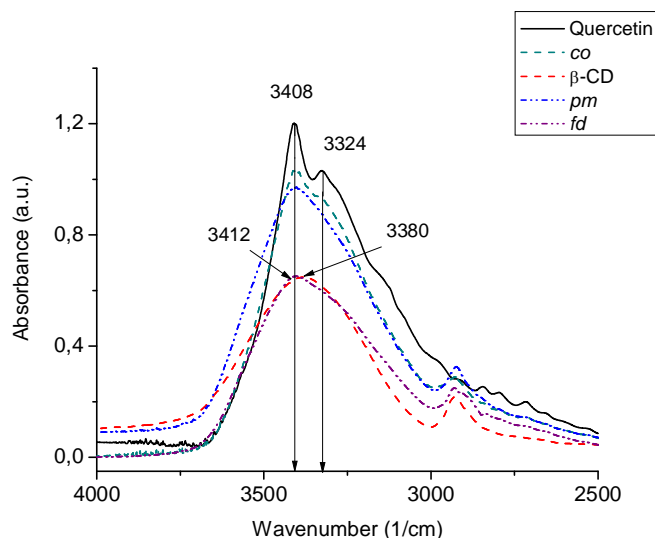


Fig. 8.1.1. FTIR spectra of pure quercetin (Q) and  $\beta$ -cyclodextrin ( $\beta$ -CD) and for the inclusion compounds of Q with  $\beta$ -CD, for the spectral domain  $4000\text{-}2500\text{ cm}^{-1}$ . Symbols: coprecipitated (*co*), freeze-dried (*fd*) and physical mixture (*pm*).

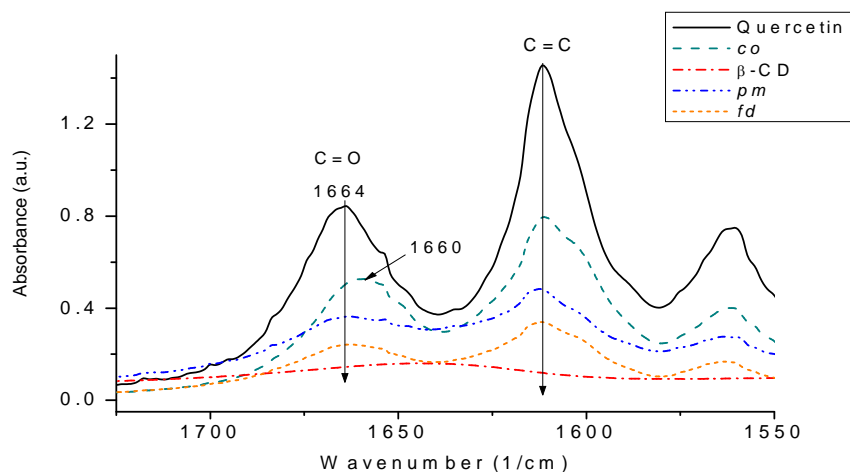
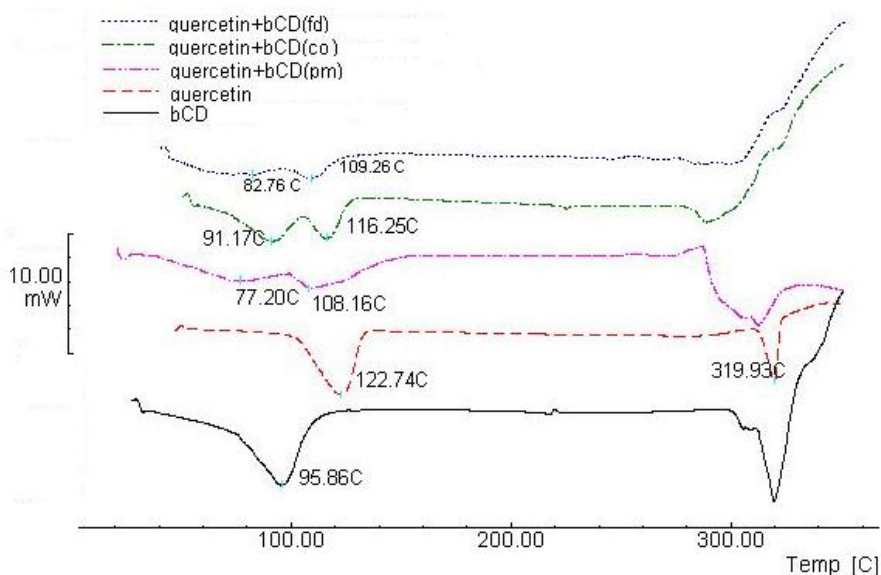


Fig. 8.1.2. . FTIR spectra of pure quercetin and  $\beta$ -cyclodextrin and for the inclusion compounds of Q with  $\beta$ -CD, for the spectral domain 1725-1550  $\text{cm}^{-1}$ .

### 8.1.2.1. 2. Differential Scanning Calorimetry (DSC)

The DSC curve for  $\beta$ -cyclodextrin shows a broad endothermic peak (Fig.8.1.3) for the temperature domain from about 74 to 118 $^{\circ}\text{C}$ , with a peak temperature of about  $95.8 \pm 1.6$   $^{\circ}\text{C}$ . The enthalpy,  $\Delta H$ , was calculated to be about.  $209.3 \pm 8.6$  J/g, and it corresponds to dehydration and loss of water molecules by evaporation of existent residual moisture (under 100 $^{\circ}\text{C}$ ), and of those included in the cavity (over 100 $^{\circ}\text{C}$ ). From 290 $^{\circ}\text{C}$  up there is a new endothermic peak, corresponding to melting followed by decomposition of  $\beta$ -cyclodextrin.



**Fig.8.1.3** DSC curves: heat flow (endothermic effects: downwards, mW, against temperature, Celsius degrees, C) for pure compounds,  $\beta$ -cyclodextrin ( $\beta$ -CD) and quercetin (Q) dihydrate, and inclusion compounds Q:  $\beta$ -CD obtained by the following preparation methods: coprecipitation (*co*) and freeze-drying (*fd*), and for the physical mixture Q:  $\beta$ -CD (*pm*).

The DSC curve of quercetin, a dihydrate, shows two endothermic processes. The first is a rather large endothermic peak at about  $122.7 \pm 1.3$  °C and corresponds to the loss of bonded water (enthalpy:  $254.2 \pm 8.8$  J/g). The second endothermic profile shows a peak temperature of  $319.9 \pm 0.8$  °C and is related to the melting of the anhydrous Q compound. The enthalpy is  $81.2 \pm 1.3$  J/g and corresponds to the melting of the Q compound, probably followed by its decomposition.

The DSC curve of the physical mixture of Q and  $\beta$ -CD shows two broad endothermic peaks between 60 and 100°C, one due to the loss of unbounded water molecules, and another for the temperature domain from 103 to 140 °C, corresponding to bonded water molecules, with  $\Delta H$  values of about  $25.6 \pm 5.3$  J/g, and about  $64 \pm 10$  J/g, respectively. The third endothermic peak, broader, begins at 287°C and corresponds to the melting of the physical mixture of Q and  $\beta$ -CD, followed by its decomposition.

The DSC curve of the inclusion compound, coprecipitated from Q and  $\beta$ -CD shows two large endothermic peaks. The first peak is characterized by a peak temperature of 91.17°C and  $\Delta H$  equal to  $68 \pm 8.3$  J/g, and the second has a peak temperature of 116.25°C and  $\Delta H$ :  $42.2 \pm 7.8$  J/g. Both peaks correspond to the loss of water molecules. The peak related to quercetin melting disappears from the thermic profile, and at about 280°C begins the decomposition of the inclusion complex.

The DSC curve of the inclusion compound of quercetin and  $\beta$ -CD, obtained by the freeze-drying method shows a single weak endothermic peak, at 109.26°C with  $\Delta H$ :  $27.1 \pm 8.2$  J/g corresponding to the loss of water molecules. The decomposition of this complex begins at about 300°C, its thermal stability being higher than for the complex quercetin:  $\beta$ -CD (*co*), thus indicating that the best method to prepare the inclusion complex is freeze-drying.

These findings could be considered as evidence for molecular interactions between the components Q and  $\beta$ -CD in the inclusion complex, thus confirming the complex formation.

### **8.1.2.1. 3 X-ray powder diffractometry**

In Fig.8.1.4 are shown the X ray powder diffraction patterns for  $\beta$ -CD, quercetin and for their inclusion complexes in the molar ratio 1: 1, prepared by two different methods, by freeze drying (*fd*, Fig.8.1.4a) and by kneading (*kn*, Fig.8.1.4b).

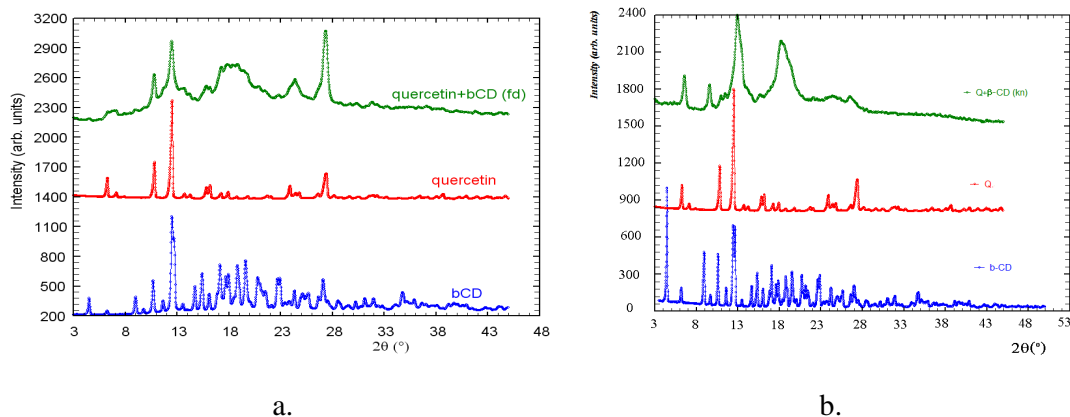


**Fig. 8.1.4.** X-ray powder diffractograms for  $\beta$ -CD, Q and their inclusion compound Q:  $\beta$ -CD, obtained by (a) freeze-drying (*fd*) and (b) kneading (*kn*) techniques.

It is evident that the X-ray diffractograms have different features for both inclusion compounds, obtained by coprecipitation (*co*) and freeze drying (*fd*), as compared to the original compounds (Q and  $\beta$ CD). These findings confirm the formation of inclusion complexes of Q and  $\beta$ CD by both techniques, *co* and *fd*.

### 8.1.2.2 The inclusion complex and the supramolecular assembly geometry

The geometry of the complex was optimized using molecular mechanics algorithm of the HyperChem program. As shown in Fig.8.1.6, the ketone groups (C=O at C4 of the C ring of quercetin) can participate in the formation of a hydrogen bond with the primary hydroxyl group located on the  $\beta$ -CD cavity.

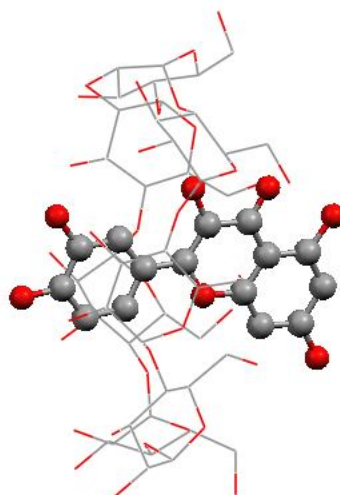
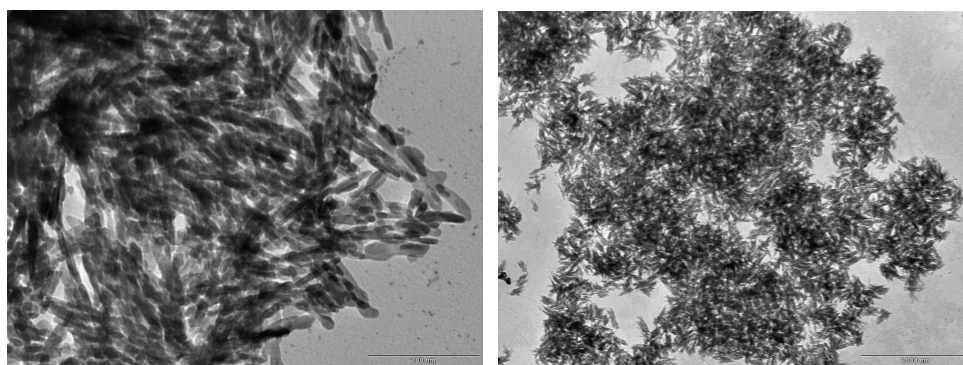


**Fig.8.1.6** Proposed molecular model for the inclusion complex formed from quercetin and  $\beta$ -cyclodextrin

### 8.1.3. Morphology and structure

Quercetin,  $\beta$ -CD and their inclusion complexes are investigated and characterized using TEM, SEM and AFM images, thus being identified different sized aggregates. TEM images (Fig.8.1.8) show a random organization of elongated, rather linear, supramolecular associations of quercetin molecules, which extend on hundreds of nanometers (Fig.8.1.8b) or even on several  $\mu\text{m}$ . All inclusion complexes containing  $\beta$ -CD and Q (obtained by kneading, coprecipitation or freeze drying techniques) show a tendency to form almost the same type of arrangements as threads, like pure quercetin, as evidenced from TEM measurements.



b.

d.

**Fig. 8.1.8.** TEM images for quercetin (a) and the inclusion complex Q:  $\beta$ -CD obtained by freeze drying (*fd*) (d)

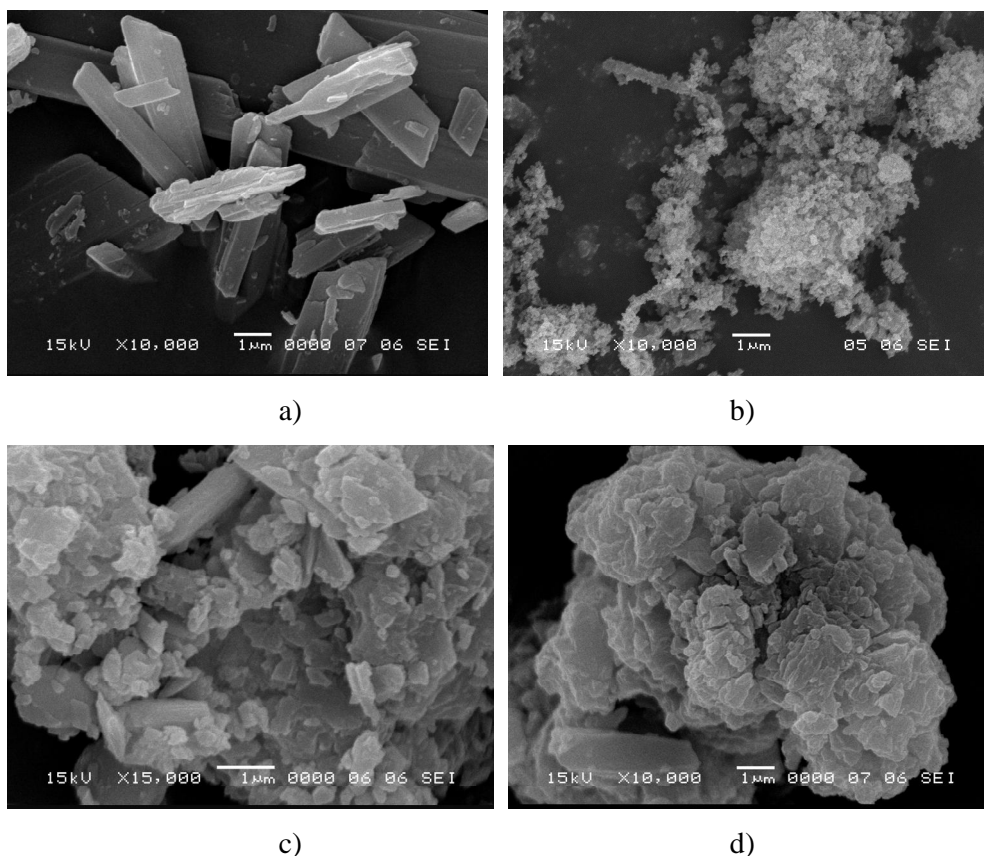


**Fig. 8.1.9.** SEM images for quercetin (a),  $\beta$ -CD (b) inclusion complex Q:  $\beta$ -CD obtained by kneading or kneading with coprecipitation (c) ) inclusion complex Q:  $\beta$ -CD obtained by freeze drying (d); Length of the bar: 1  $\mu$ m.

In the SEM images (Fig. 8.1.9), the inclusion complexes formed by  $\beta$ -CD and Q (Fig. 8.1.9c and d) show particles with comparable morphology, practically independent of the preparation technique (kneading, respectively freeze drying in Fig. 8.1.9d). The morphology and shape of these particles are quite different from those corresponding to the pure components, quercetin or  $\beta$ -CD, revealing a different structure in solid phase, on account of molecular interactions in the lattice of the inclusion complexes, in agreement with TEM observations.

### 8.1.6.2. Experimental estimation of the equilibrium constant

Some of the UV-VIS spectra, for the aqueous alcoholic quercetin solutions with  $\beta$ CD in different ratios, are given in Fig.8.1.13 for pH = 3. In all the solutions two peaks are present, with maxima at 372 and 255 nm. The absorbance at the maxima presented a general increasing trend with increasing  $\beta$ CD concentrations. Three different aqueous media, namely

pH 3, unbuffered (pH 5.5) and pH 7.4, have been used to vary the environmental conditions and the interaction between BCD and Q molecules.

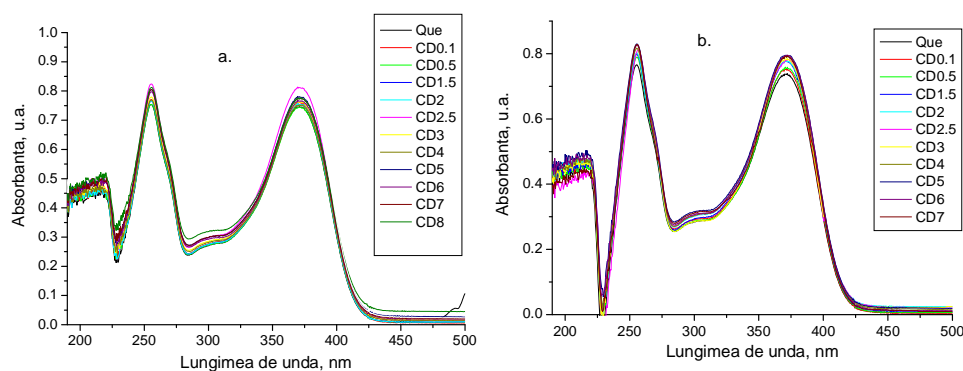


**Fig.8.1.13.** Optical spectra of 0.04 Q solutions with variable  $\beta$ CD contents at pH = 3 (citrate buffer), 2 min. after mixing (a), and after 24 h (b).

The equilibrium constant  $K$  of the molecular host-guest complex formation was estimated using the Benesi-Hildebrand method in 4 versions [566], for the two absorption peaks. In Tabl 8.1.2, the values obtained by us from different graphical treatments are summarized.

**Table 8.1.2.** Estimated values for the binding equilibrium constant for the  $\beta$ CD-Q complex

Method	371 nm absorption band	256 nm absorption band
<b>pH = 3</b> , after 2 min. from ec.(2)	300 ( $r = 0.558$ )	150 ( $r = 0.434$ )
<b>pH = 3</b> , after 24 h		
from eq. (1)	$725 \pm 50$ (0.996)	$1100 \pm 250$ (0.931)
from eq. (2)	$760 \pm 100$ (0.995)	$650 \pm 170$ (0.973)
from eq. (3)	$750 \pm 70$ (0.967)	$1040 \pm 250$ (0.768)
from eq. (4)	$810 \pm 100$ (0.995)	$810 \pm 220$ (0.973)
Average	$750 \pm 150$	$900 \pm 400$
Average from 2 max	820	
<b>pH = 5.5</b>		
from eq. (1)	$710 \pm 70$ (0.990)	$570 \pm 170$ (0.858)
from eq. (2)	$610 \pm 100$ (0.990)	$530 \pm 160$ (0.959)
from eq. (3)	$740 \pm 90$ (-0.928)	$670 \pm 190$ (-0.711)
from eq. (4)	$680 \pm 110$ (0.990)	$710 \pm 210$ (0.959)
Average	$680 \pm 150$	$620 \pm 230$
Average from 2 max	650	

At pH 7.4 the partial ionization of quercetin and the low stability of its anionic form preclude the estimation of reliable  $K$  values.

From the estimated binding constant  $K$ -values, the Gibbs free energy (free enthalpy) of formation [524, 525] for the host-guest molecular complex can be calculated.

The obtained values are:  $-16.6$  kJ/mol (pH = 3),  $-16.0$  kJ/mol (pH = 5.5).

## 8.2. SUPRAMOLECULAR STRUCTURES FORMED FROM $\beta$ -CYCLODEXTRIN AND $\alpha$ -LIPOIC ACID

### 8.2.3. Physicochemical characterization of the inclusion complex formed from lipoic acid (LA) and $\beta$ -cyclodextrin [533-536]

- FTIR spectroscopy

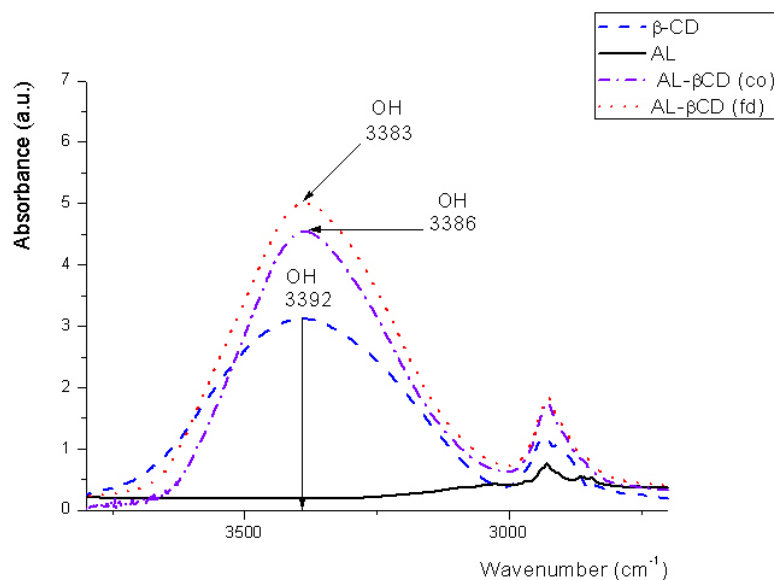


**Fig. 8.2.2** FTIR spectra of pure lipoic acid and  $\beta$ -cyclodextrin, and for inclusion complexes of LA with  $\beta$ -CD, in the spectral domain  $3800$ - $2700$   $\text{cm}^{-1}$ . Symbols: coprecipitated (*co*), freeze dried (*fd*).

The stretching frequency of the O-H group, located at  $\sim 3392$   $\text{cm}^{-1}$  in pure  $\beta$ -CD, is shifted at  $3386$  (*co* product) and  $3383$   $\text{cm}^{-1}$  (*fd* product), respectively because of the increased number of hydrogen bonds during the complexation process. But also the expulsion of water molecules from the  $\beta$ -CD cavity.

In the spectral region  $1800$ - $1500$   $\text{cm}^{-1}$  some changes also occur after complexation.

-  $\nu_{as}(C=O)$  of lipoic acid is shifted toward higher frequencies, probably because of the destruction of the structure with strong hydrogen bonds in the non complexed substance, after the formation of the inclusion compound with  $\beta$ -cyclodextrin.

-  $\nu(OH)$  (bending mode) of  $\beta$ -CD is shifted to a lower frequency, which could be explained by the formation of new hydrogen bonds between  $\beta$ -CD and LA.

## 8.2.4 STRUCTURE OF THE CRYSTAL LATTICE FORMED BY THE INCLUSION COMPLEX OF LIPOIC ACID WITH $\beta$ -CYCLODEXTRIN

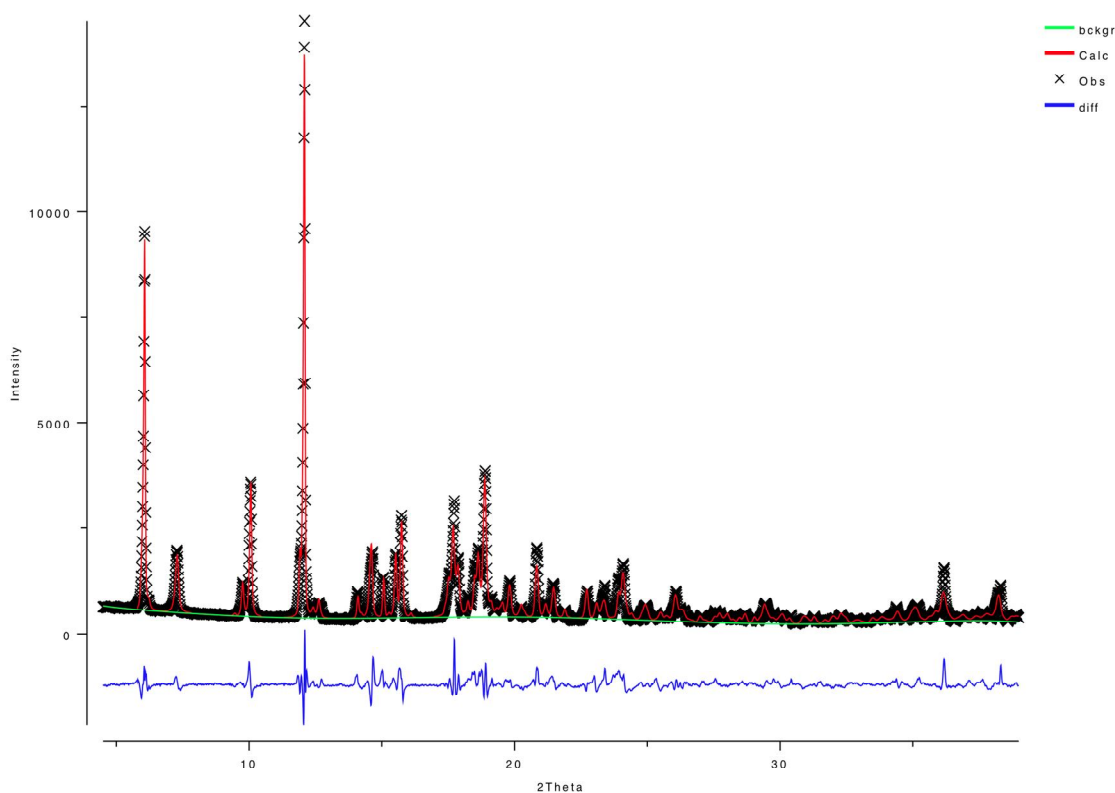


Figure 8.2.4.3. X-ray powder diffraction patterns of the (1:1)  $\beta$ -CD-LA inclusion complex; experimental spectrum (x x x x), final calculated spectrum after refinement (line) and the difference experimental- calculated spectrum (line, down).

In order to build the model of the inclusion complex, we used the reference structures from Cambridge Structural Database [557-559].

### 8.2.4.3. Molecular packing and hydrogen bonds in the inclusion complex $\beta$ -CD – lipoic acid (1:1)

**Table 8.2.4.2.** The characteristics of the  $\beta$ -CD molecule. D= distances between atoms O4(G<sub>n</sub>)...O4(G<sub>n+1</sub>) ;  $\varphi$  = angles between atoms O4(G<sub>n-1</sub>)...O4(G<sub>n</sub>)...O4(G<sub>n+1</sub>); d=deviations from the least-square plane through the seven O4(G<sub>n</sub>) atoms;  $\alpha$ =dihedral angle between the O4(G<sub>n</sub>) plane and the least-square plane through C2(G<sub>n</sub>),C3(G<sub>n</sub>), C5(G<sub>n</sub>) and O5(G<sub>n</sub>); D3=intramolecular distances between atoms O3(G<sub>n</sub>)...O2(G<sub>n+1</sub>). Torsion angle  $\tau_a$ =O5(G<sub>n</sub>)-C5(G<sub>n</sub>)-C6(G<sub>n</sub>)-O6(G<sub>n</sub>) and  $\tau_b$ =C4(G<sub>n</sub>)-C5(G<sub>n</sub>)-C6(G<sub>n</sub>)-O6(G<sub>n</sub>).

Resi- duum	D(Å)	$\varphi$ (°)	d(Å)	$\alpha$ (°)	D3(Å)	$\tau_a$ (°)	$\tau_b$ (°)
G1	5.44(4)	128.0(9)	0.123(14)	66.3(5)	3.10(3)	93.1(18)	-135.2(19)
G2	5.58(4)	127.8(7)	-0.07(3)	88.7(10)	2.52(4)	-104(3)	29(3)
G3	5.38(5)	101.8(7)	0.12(3)	89.0(13)	3.23(4)	-120(4)	11(4)
G4	4.71(5)	153.8(10)	0.30(4)	81.9(11)	2.90(4)	-38(3)	93(3)
G5	5.22(5)	129.2(9)	-0.63(3)	69.7(11)	3.33(3)	-157(3)	-33(4)
G6	5.55(3)	98.8(6)	0.41(3)	88.3(11)	2.74(3)	-168(3)	-45(3)
G7	4.42(3)	150.8(7)	0.00(3)	76.0(11)	2.99(2)	-54(4)	75(4)

The seven glycosidic O4(G<sub>n</sub>) atoms in  $\beta$ -CD-LA (1:1) form a distorted heptagon, given the large deviations of the interatomic distances (4.42 – 5.58 Å) and interatomic angles (99 – 154°) (Table 8.2.4.2) from the values of 4.38 Å and 128.6° in an ideal non-distorted heptagon.

The seven glucose units have slightly distorted chair conformations, with puckering theta angles between 0 – 7°, originating from the  $\beta$ -CD model used to construct the  $\beta$ -CD-LA inclusion compound.

The oxygens O6 of G<sub>2</sub>, G<sub>3</sub>, G<sub>4</sub>, G<sub>6</sub>, G<sub>7</sub> are outside the cyclodextrin cavity and the O6 of G<sub>1</sub> and G<sub>5</sub> point into the macrocycle cavity and narrow down opposite sides of the  $\beta$ -CD primary face.

In general, hydrogen bonds with O6(G<sub>n</sub>) of neighboring cyclodextrin molecules are formed if the O6(G<sub>n</sub>) are in the same position as the C2C3C5O5 plane. The fact that no O6 oxygen atom in the  $\beta$ -CD-LA inclusion complex satisfies these criteria explains the presence of only one H bond between the O6(G<sub>4</sub>) – O6(G<sub>7</sub>) of neighboring cyclodextrins and their extensive involvement in the intra-molecular hydrogen bonding (Table 8.2.4.3).

**Table 8.2.4.3.** Intramolecular hydrogen-bonding distances. The first index is related to the usual notation for the glycoside unit as in the Fig. 8.2.4.1. The second index corresponds to the glycoside unit number in the  $\beta$ -CD macrocycle.

Primary –OH groups of $\beta$ -CD		Secondary –OH groups of $\beta$ -CD	
Bonded atoms	Length (Å)	Bonded atoms	Length (Å)
O <sub>62</sub> – O <sub>43</sub>	2.32	O <sub>22</sub> – O <sub>31</sub>	3.10
O <sub>62</sub> – O <sub>53</sub>	2.45	O <sub>23</sub> – O <sub>32</sub>	2.52
O <sub>63</sub> – O <sub>44</sub>	2.75	O <sub>25</sub> – O <sub>34</sub>	2.90
O <sub>63</sub> – O <sub>54</sub>	2.70	O <sub>27</sub> – O <sub>36</sub>	2.74
O <sub>64</sub> – O <sub>45</sub>	2.84	O <sub>21</sub> – O <sub>37</sub>	2.99
O <sub>65</sub> – O <sub>46</sub>	2.88		
O <sub>65</sub> – O <sub>56</sub>	2.38		
O <sub>66</sub> – O <sub>47</sub>	2.71		
O <sub>66</sub> – O <sub>57</sub>	2.44		
O <sub>67</sub> – O <sub>57</sub>	2.83		

The cyclodextrins are packed in the channel-type, head-to-head arrangement, the cyclodextrin molecules form tubular dimers in which the CD's primary rims are linked together by one hydrogen bond and few O6 ... O6 intermolecular close contacts. The two secondary rims of each dimer are also involved in two H-bond interactions with secondary rims of adjacent dimers

Three water molecules (O71 – O73) contribute to the H-bonding between the primary faces of the  $\beta$ -CD dimers, and one water molecule (O74) to the H-bonding of the dimers corresponding secondary faces. The channel packing of the CD molecules with the water molecules present in between the CD layers is shown in Figure 8.2.4.5.

#### 8.2.4.4. Mode of inclusion and guest conformation.

The LA molecule is included into the cyclodextrin cavity through the primary rim (narrow face) with the five-membered ring close to the macrocycle O4(G<sub>n</sub>) plane. The S4 atom of the guest LA molecule is located at a distance  $d = 0.406(15)$  Å from this plane. The LA molecule is connected by one C-H...O hydrogen bond to the cyclodextrin molecule in which it is docked and its carboxyl oxygen O11 is hydrogen bonded to one water molecule

(O72).

In addition, the carboxyl oxygen O11 of LA is in close contact with the G<sub>2</sub> glucose of a neighboring cyclodextrin molecule. When viewed down the *b*-axis, two symmetry-related LA molecules have their fatty acid chains outside the hydrophobic CD cavity and they are filling the space between the slightly shifted CDs of a dimer (Fig. 8.2.4.4b, 8.2.4.5b).

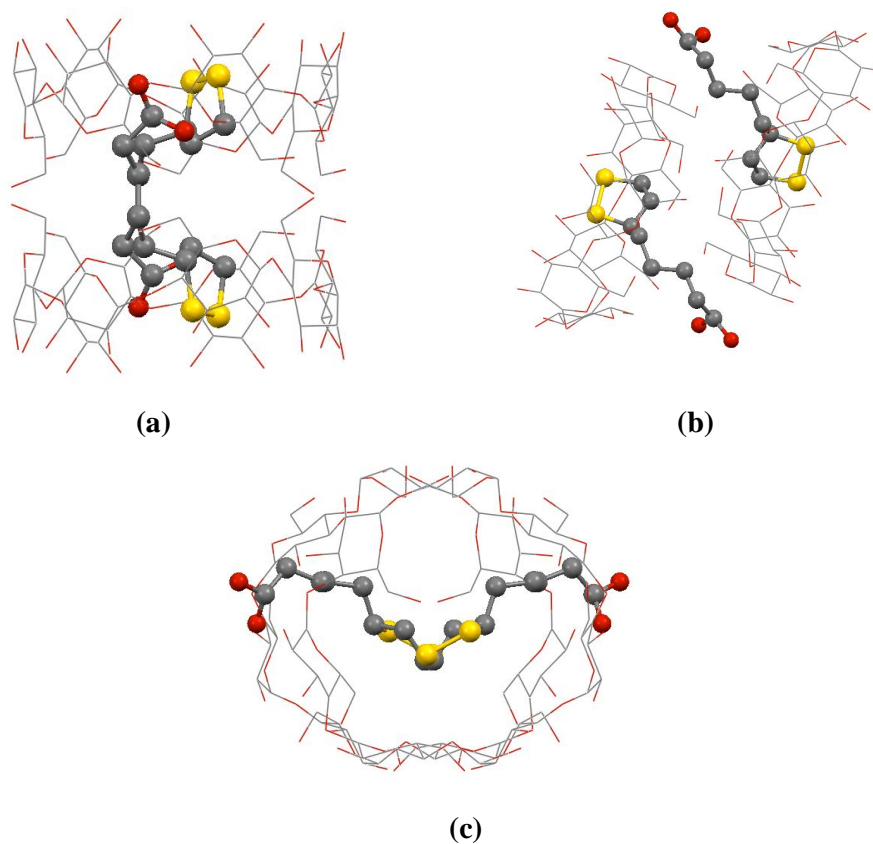
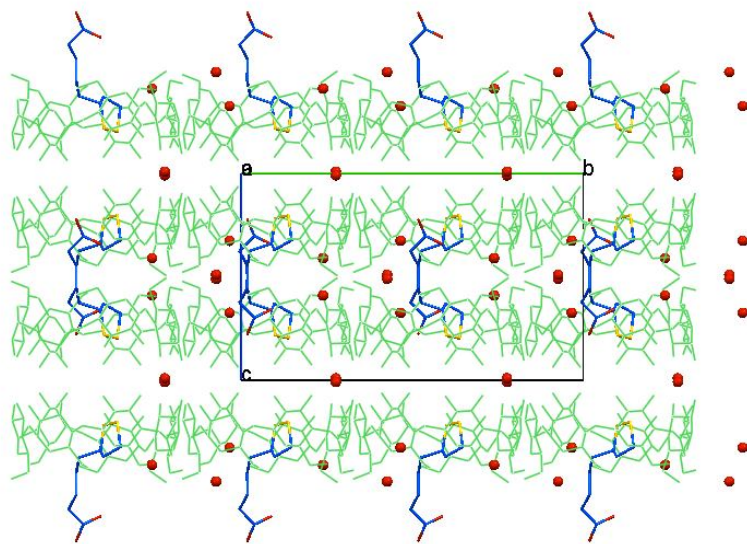
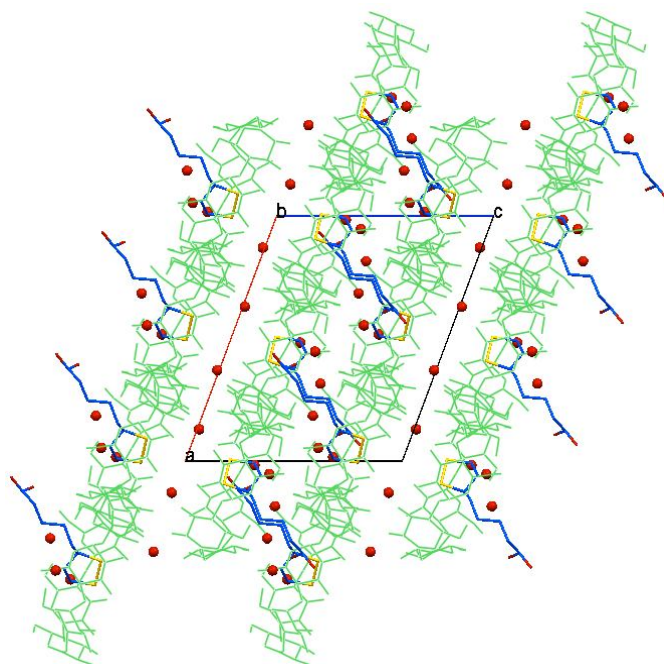


Fig. 8.2.4.4. Molecular packing of the  $\beta$ -CD dimers with included lipoic acid (LA), viewed along the *a*-axis (a), *b*-axis (b) and *c*-axis (c), respectively. The H atoms and the O water atoms were excluded for clarity.

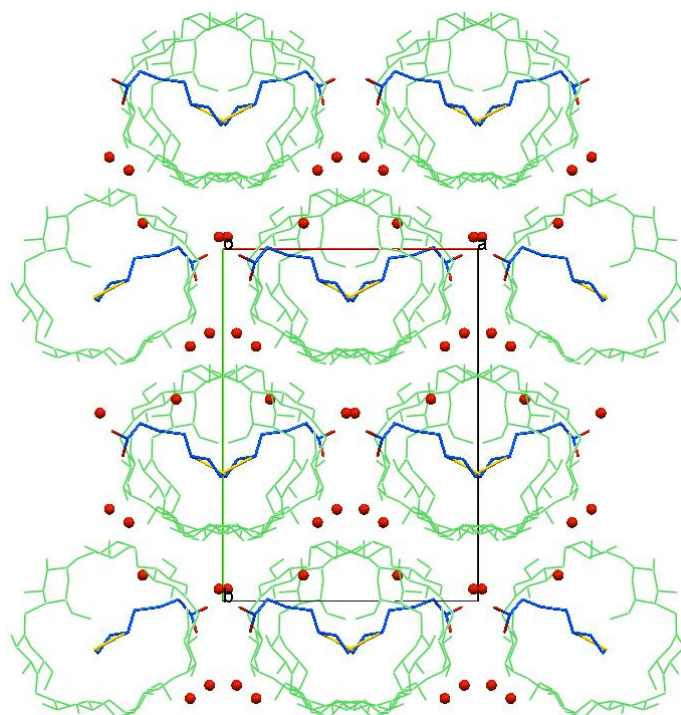
The channel-like packing of the LA inclusion complex in  $\beta$ -CD is stabilized by guest-host hydrogen bonding and close contacts, the  $\beta$ -CD -  $\beta$ -CD intermolecular interactions and H-bonding involving the water molecules.



(a)



(b)



(c)

Fig. 8.2.4.5. Molecular packing of the  $\beta$ -CD-LA inclusion complex, viewed along the  $a$ -axis (a),  $b$ -axis (b) and  $c$ -axis (c), respectively. The H atoms were excluded for clarity.

## 9. GENERAL CONCLUSIONS

- The interfacial tension in two phase systems (benzene-water), in presence of sodium cholate (NaC) was measured against the surfactant concentration at different temperatures, and critical micelle concentration and thermodynamic parameters of adsorption were determined. From the analysis of experimental data, it was evident that cholate geometry and hydrophilicity have a considerable effect on the properties of adsorbed sodium cholate films and on the behavior of micelles formation, with major impact on the stability of micellar systems.
- The adsorption mechanism for two local anesthetics, dibucaine and tetracaine and for stearic acid was studied from aqueous solution to the oil-water interface. In order to describe their adsorption kinetics, a new theoretical model was developed, and a new kinetic equation for diffusion controlled adsorption was proposed. This original research demonstrates the diversity of analysis possibilities of molecular suprastructures oriented in Langmuir films.
- The semi empirical SCF-MO (AM1 and PM3) calculations for the three carotenoids investigated give general results similar to those indicated by HMO calculations. The calculated dipole moments of the polar groups were correlated with thermodynamic surface characteristics and conclusions were drawn regarding molecular orientation in the condensed monolayer.
- The stability of mixed DPPC Langmuir films with procaine at the air/water interface is much higher than that of pure DPPC nanolayers, as shown by the increased value of the collapse pressure of the mixed film.
- The surface of LB films of pure DPPC and mixed with procaine, transferred on aluminum support, was visualized by AFM, for the first time worldwide. They offer models for cell biomembranes. The high stability of LB films and Langmuir nanolayers may be useful in various applications in medicine, pharmacy and biology.
- Stable gold and silver colloidal solutions were prepared and characterized by UV-Vis spectroscopy and TEM imaging. By means of these techniques the self aggregation / selfassembly of metal nanoparticles under the influence of biologically active compounds (amino acids).
- Our data show that amino acids binding to gold nanoparticles can lead to well organized assemblies, particularly for amino acids having functional groups, such as amine, imidazole, thiol or thioether, in addition to the  $\alpha$  amine function. The affinity of gold

nanoparticles for amino acids may lead to the development of new detection methods for analysis, medical diagnosis and biosensors, and to potential applications in controlled drug release systems, as well as for the synthesis of nanostructured biomaterials with important implications in nanoscience and nanotechnology.

- Films of the storage protein from aleurone cells of barley (PAC) were investigated, after adsorption on solid support, by AFM. The AFM images show nanometric details on the surface of protein films, which can suggest the presence of a long range order, due to electrostatic effects and to the attraction between support and protein. The globular PAC protein can be a starting point for generating new supramolecular materials, necessary in molecular nanobiotechnology and for natural membrane biomimetics.
- From the investigation of melatonin effect on BSA protein at fluid interfaces, such as air/aqueous solution, we found that melatonin exerts a substantial stabilizing effect on interfacial BSA films, self assembled at the interface. Thus, it can act as a protective agent on macromolecules in vitro and in vivo by specific physicochemical interactions with biomolecules, such as BSA and / or their biologically active assemblies. Consequently, melatonin can facilitate the inhibition of biomolecules peroxidation by increasing the stability of supramolecular assemblies.
- AFM technique allows the visualization of assemblies of collagen with cancer drugs and to determine their morphology and surface roughness. These systems could also be appropriate to produce biological surfaces with biomedical applications, for drugs releasing at their place of action and for the construction of biosensors.
- By AFM imaging, on the surface of maize starch granules numerous structures were found, protrusions (particles), pores or low areas and cracks, which have a wide range of sizes. The apparition of small, spherical protrusions can be related to highly branched (ramified) amylopectin molecules, in substantial agreement with the blocklets model. Larger particles were also vusalized, representing various associations of amylopectin with amylose and other components of the granule surface.
- The investigation of maize and potatoes starch using scanning electron microscopy evidenced the shape, surface morphology and size of starch granules. Using SEM images, the size distribution of granules was determined, and compared for different samples. These investigations will contribute to the characterization of starch granules, used as raw material for the production of biodegradable plastics.

- The inclusion complexes of quercetin (Q) and  $\beta$ -cyclodextrin ( $\beta$  CD) were prepared by coprecipitation and freeze drying techniques, which were optimized for complexation as good as possible. FTIR, X-rays diffraction and DSC are adequate and complementary methods, providing evidence of Q molecular encapsulation in the  $\beta$ -CD nanocavity, in solid state.
- A model for the inclusion complex of Q in  $\beta$ -CD, obtained by molecular modeling suggests quercetin being closed in the hydrophobic nanocavity of  $\beta$ -CD, mainly by interaction of its ketone group at C4 with the OH groups of the nanocavity of  $\beta$ -CD. TEM, SEM and AFM imaging was used to evidence the changes in physical aspect, starting with the initial pure compounds, Q and  $\beta$ -CD, to the inclusion complexes obtained in solid state by different methods.
- Our results can be a direct contribution to molecular encapsulation of quercetin in  $\beta$ -cyclodextrin, which can improve stability and bioavailability of quercetin, taking into account the fact that quercetin is an important nutritional supplement with proven health benefits.
- Spectroscopic research on the molecular host-guest complex (1:1 stoichiometry) of  $\beta$ CD and Q allow estimating the equilibrium constant of formation, K, in aqueous solution at various pH values, and hence the Gibbs free energy and the enthalpy of formation of the inclusion complex from pure initial substances. The negative  $\Delta G^0$  value is the result of enthalpy variation, while the contribution of entropy is not essential. The main driving force for the complex formation could be related to the replacement of water molecules in the hydrophobic cavity of  $\beta$ -CD (host molecules) with quercetin guest molecules.
- The inclusion compound of  $\alpha$ -lipoic acid with  $\beta$ -cyclodextrin was obtained by the freeze-drying and coprecipitation techniques. DSC investigations reveal a good thermal stability of the inclusion compound. Along with the FTIR investigations, it is demonstrated the existence of molecular interactions between LA and  $\beta$ -CD, supporting the complex formation.
- The crystalline structure of the lattice, generated by the inclusion complex, consisting of LA and  $\beta$ -CD, is deciphered for the first time in literature, in this Ph.D. Thesis. The crystalline structure is deduced from data furnished by high resolution X-ray powder diffraction (XRPD), with a laboratory X-rays source, combined with techniques of advanced data refinement.

## SELECTED REFERENCES

- [3] E. Chifu, "Chimia Coloizilor și a Interfețelor", **Editori:** M. Tomoaia-Cotisel, I. Albu, A. Mocanu, M. Salajan, E. Gavrilă, **Cs. Racz**, Presa Universitară Clujeană, Cluj-Napoca, **2000**, pp. 400.
- [4] E. Chifu, M. Tomoaia-Cotisel, I. Albu, A. Mocanu, M. Salajan, **Cs. Racz**, V.D. Pop, "Metode Experimentale in Chimia si Biofizica Coloizilor și a Interfețelor", Presa Universitara Clujeana, Cluj-Napoca, **2004**, pp. 175.
- [90] D. M. Small, *Physical Chemistry of Cholanic Acids* in "The Bile Acids - Chemistry, Physiology and Metabolism", Eds., P. P. Nair, D. Kritchevsky, Plenum Press, New York, **1971**, p. 255.
- [92] J. Ulmius, G. Lindblom, H. Wennerstrom, L. B. Johansson, K. Fontell, O. Soderman, G. Arvidson, *Biochemistry*, **21**, 1553, 1982.
- [94] S. Ross, J. P. Olivier, *J. Phys. Chem.*, **63**, 1671, 1959.
- [96] R. Zana, D. Guveli, *J. Phys. Chem.*, **89**, 1687, 1985.
- [123] J. Zsakó, A. Mocanu, **Cs. Racz**, K. Racz, E. Chifu, *Stud. Univ. Babeş-Bolyai, Chem.*, **42** (1-2), 37, 1997.
- [124] J. Zsakó, M. Tomoaia-Cotisel, A. Mocanu, **Cs. Racz**, E. Chifu, *J. Romanian Colloid and Surface Chem. Assoc.*, **2** (3-4), 37, 1997.
- [177] M. Tomoaia-Cotisel, J. Zsakó, A. Mocanu, M. Salajan, **Cs. Racz**, S. Bran., E. Chifu, *Stud. Univ. Babeş-Bolyai, Chem.*, **48** (1), 201, 2003.
- [190] G. Tomoaia, M. Tomoaia-Cotisel, **Cs. Racz**, C. Ispas, C. Floare, *Stud. Univ. Babeş-Bolyai, Chem.*, **50** (1), 47, 2005.
- [207] M. Tomoaia-Cotișel, **Cs. Racz**, G. Tomoaia, C. Floare, R. Totos, L. Bobos, O. Pascu and A. Dumitru, *Stud. Univ. Babeş-Bolyai, Chem.*, **50** (1), 39, 2005.
- [208] O. Horovitz, G. Tomoaia, **Cs. Racz**, A. Mocanu, L. Bobos, M. Tomoaia-Cotisel, *Central European Journal of Chemistry*, **4** (3), 489, 2006.
- [249] M. Tomoaia-Cotisel, V-D. Pop, Gh. Tomoaia, A. Mocanu, **Cs. Racz**, C.R. Ispas, O. Pascu, O.C. Borostean, *Stud. Univ. Babeş-Bolyai, Chem.*, **50** (1), 23, 2005.
- [328] O. Horovitz, A. Mocanu, Gh. Tomoaia, M. Crisan, L.-D. Bobos, **Cs. Racz**, M. Tomoaia-Cotisel, *Stud. Univ. Babeş-Bolyai, Chem.*, **52** (3), 53, 2007.
- [329] O. Horovitz, M. Tomoaia-Cotisel, **Cs. Racz**, Gh. Tomoaia, L.-D. Boboș, A. Mocanu, *Stud. Univ. Babeş-Bolyai, Chem.*, **54** (3), 89, 2009.
- [337] A. Mocanu, G. Tomoaia, M. Tomoaia-Cotisel, **Cs. Racz**, C.R. Ispas, J. Zsakó, *Stud. Univ. Babeş-Bolyai, Chem.*, **49** (1), 29 (2004).

- [359] M. Tomoaia-Cotisel, A. Tomoaia-Cotisel, T. Yupsanis, Gh. Tomoaia, I. Balea, A. Mocanu and **Cs. Racz**, *Rev. Roum. Chim.*, **51**, 1201, 2006.
- [432] M. Tomoaia-Cotisel, N. Cioica, C. Cota, **Cs. Racz**, I. Petean, L. D. Bobos, A. Mocanu, O. Horovitz, *Stud. Univ. Babeş-Bolyai, Chem.*, **55** (2), 313, 2010.
- [433] M. Tomoaia-Cotisel, **Cs. Racz**, N. Cioica, C. Cota, I. Petean, L.D. Bobos, A. Mocanu and O. Horovitz, "Healthy Nutrition and Public Health", IC-HNPH – 2011, Transilvania University of Brasov, Romania, May 13-16, **2011**.
- [489] I. Bratu, Gh. Tomoaia, Gh. Borodi, I. Daian, **Cs. Racz**, A. Mocanu, I. Kacso, Sz. Santa, M. Tomoaia-Cotisel, *The fifth Conference "Isotopic and Molecular Processes"*, PIM 2007, Cluj-Napoca, September 20-22, **2007**.
- [491]. Gh. Borodi, I. Bratu, **Cs. Racz**, Gh. Tomoaia, I. Daian, Sz. Santa, A. Mocanu, I. Kacso, M. Tomoaia-Cotisel, *The fifth Conference "Isotopic and Molecular Processes"*, PIM 2007, Cluj-Napoca, September 20-22, **2007**.
- [492] M. Tomoaia-Cotisel, **Cs. Racz**, Gh. Borodi, Gh. Tomoaia, I. Bratu, I. Kacso, Sz. Santa, A. Mocanu, The 15th International Cyclodextrin Symposium", Vienna, May 9-12, **2010**.
- [494] **Cs. Racz**, Gh. Borodi, Gh. Tomoaia, I. Bratu, I. Kacso, A. Mocanu, M. Tomoaia-Cotisel, "The 15th international cyclodextrin symposium", Vienna, May 9-12, **2010**.
- [495]. **Cs. Racz**, M. Tomoaia-Cotisel, in the International Conference, "Healthy Nutrition and Public Health", IC-HNPH-2011, Transilvania University Brasov, Romania, May 13-16, **2011**.
- [496] **Cs. Racz** and Maria Tomoaia-Cotisel, The 10<sup>th</sup> International Conference on Colloid and Surface Chemistry, "Dunarea de jos" University of Galati, Galati, June 9-11, **2011**.
- [524] M. Tomoaia-Cotisel, O. Horovitz, A. Mocanu, I. Albu, **Cs. Racz**, "Termodinamica Chimica in Aplicatii Numerice, Diagrame si Teste", Presa Universitară Clujeană, Cluj-Napoca, **2007**, pp. 210.
- [525] M. Tomoaia-Cotisel, O. Horovitz, A. Mocanu, I. Albu și **Cs. Racz**, "Termodinamica Chimica in Aplicatii Numerice, Diagrame si Teste", *Editia a II-a, revăzută și adăugită*, Presa Universitară Clujeană, Cluj-Napoca, **2008**, pp. 226.
- [533] **Cs. Racz**, I. Bratu, Gh. Borodi, Gh. Tomoaia, M. Tomoaia-Cotisel, A. Mocanu, I. Kacso and Sz. Santa, "*The 2<sup>nd</sup> International Conference - Advanced Spectroscopies on Biomedical and Nanostructured Systems*", Cluj-Napoca, NANOSPEC, September 3-6, **2006**.
- [534] I. Bratu, Gh. Borodi, **Cs. Racz**, Gh. Tomoaia, M. Tomoaia-Cotisel, A. Mocanu, I. Kacso and Sz. Santa, "*The First International Symposium on Supramolecular Chemistry*", Faculty of Chemistry and Chemical Engineering, Cluj-Napoca, April, 12-15, **2007**.
- [535] **Cs. Racz**, I. Albu, M. Tomoaia-Cotisel, A. Mocanu, "*Micro Symposium – In memoriam Profesor Mathe*", Faculty of Chemistry and Chemical Engineering, Cluj-Napoca, 19 May, **2007**.

- [536] Gh. Borodi, **Cs. Racz**, Sz. Santa, I. Bratu, I. Kacso, A. Mocanu and M. Tomoaia-Cotisel, *The Conference "Processes in Isotopes and Molecules"*, PIM 2011, Cluj-Napoca, September 29-October 1, **2011**.
- [557] F. H. Allen, O. Kennard, *Chem. Des. Autom. News*, **8**, 31, 1993.
- [558] T. Steiner, J. Koellner, *J. Am. Chem. Soc.* **114**, 5122, 1994.
- [559] R.M. Stroud, C.H. Carlisle, *Acta Cryst. B*, **28**, 307, 1972.
- [566] **Cs. P. Racz**, R.-D. Pasca, Sz. Santa, I. Kacso, A. Mocanu, O. Horovitz and M. Tomoaia-Cotisel, *Rev. Chim. (Bucuresti)*, **62** (10), 2011 (*in press*).
- [571] M. Tomoaia-Cotișel, Gh. Tomoaia, **Cs. Racz**, A. Mocanu, C.R. Ispas, M.I. Sălăjan, I.Hălăciugă, Proceedings of the 8<sup>th</sup> Symposium on Colloid and Surface Chemistry, Galați, June 3-5, 2005, 4 pages.
- [576] L.-D. Bobos, Gh. Tomoaia, **Cs. Racz**, A. Mocanu, O. Horovitz, I. Petean, M. Tomoaia-Cotisel, *Stud. Univ. Babeș-Bolyai, Chem.*, **53** (4), 99-110 (2008).